ChemComm

FEATURE ARTICLE

View Article Online
View Journal | View Issue

Cite this: *Chem. Commun.*, 2023, **59**, 13800

Precision nanoengineering for functional self-assemblies across length scales†

Nonappa

As nanotechnology continues to push the boundaries across disciplines, there is an increasing need for engineering nanomaterials with atomic-level precision for self-assembly across length scales, *i.e.*, from the nanoscale to the macroscale. Although molecular self-assembly allows atomic precision, extending it beyond certain length scales presents a challenge. Therefore, the attention has turned to size and shape-controlled metal nanoparticles as building blocks for multifunctional colloidal self-assemblies. However, traditionally, metal nanoparticles suffer from polydispersity, uncontrolled aggregation, and inhomogeneous ligand distribution, resulting in heterogeneous end products. In this feature article, I will discuss how virus capsids provide clues for designing subunit-based, precise, efficient, and error-free self-assembly of colloidal molecules. The atomically precise nanoscale proteinic subunits of capsids display rigidity (conformational and structural) and patchy distribution of interacting sites. Recent experimental evidence suggests that atomically precise noble metal nanoclusters display an anisotropic distribution of ligands and patchy ligand bundles. This enables symmetry breaking, consequently offering a facile route for two-dimensional colloidal crystals, bilayers, and elastic monolayer membranes. Furthermore, inter-nanocluster interactions mediated *via* the ligand functional groups are versatile, offering routes for discrete supracolloidal capsids, composite cages, toroids, and macroscopic hierarchically porous frameworks. Therefore, engineered nanoparticles with atomically precise structures have the potential to overcome the limitations of molecular self-assembly and large colloidal particles. Self-assembly allows the emergence of new optical properties, mechanical strength, photothermal stability, catalytic efficiency, quantum yield, and biological properties. The self-assembled structures allow reproducible optoelectronic properties, mechanical performance, and accurate sensing. More importantly, the intrinsic properties of individual nanoclusters are retained across length scales. The atomically precise nanoparticles offer enormous potential for next-generation functional materials, optoelectronics, precision sensors, and photonic devices.

Received 5th May 2023,
Accepted 17th October 2023

DOI: 10.1039/d3cc02205f

rsc.li/chemcomm

1. Introduction

Achieving atomic precision across length scales is one of the fundamental challenges in modern nanotechnology. The future of optoelectronics, catalysis, biosensing, nanomedicine, and solutions for environmental challenges relies heavily on the ability to fabricate materials with highly precise structures and reproducible properties.[1–4] Such precision could offer programmable control over the shape, strength, conductivity, mechanical properties, and optical responses with high sensitivity.[5–7] While the potential benefits are clear, methods that allow atomic precision at the macroscopic scale are limited. Nevertheless, several attempts have been made to fabricate precise structures across length scales in recent years.[8] Large-scale three-dimensional (3D) crystals can be considered atomically precise macroscopic objects. However, crystals have limitations due to their poor mechanical properties. Notably, recent reports have demonstrated mechanically strong and flexible crystals of small molecules.[9] Furthermore, reversible two-dimensional (2D) polymer sheets have been demonstrated using the photochemical polymerization of monomer crystals.[10] The above reports are limited to certain molecules or materials under highly controlled and narrow experimental conditions. Notably, building materials atom by atom is a laborious way to produce structures in scalable quantities.

Molecular engineering is a well-established area of research. It allows precise control over the structure, functional groups, geometry, and directional interactions of molecular building blocks for the design and fabrication of materials, and systems with specific properties and functions.[11,12] It focuses on manipulating molecular properties, behaviour, and interactions to improve or fabricate new materials and their applications.

Facutly of Engineering and Natural Sciences, Tampere University, FI-33720, Tampere, Finland. E-mail: nonappa@tuni.fi

† Dedicated to Professor Olli Ikkala on the occasion of his 70th Birthday.

Therefore, molecular engineering has contributed tremendously to the success of molecular self-assembly, offering a wide range of morphologically distinct functional architectures.[13,14] Despite huge success in molecular self-assembly, obtaining large-scale structures with high precision is challenging.[15] Furthermore, achieving strictly monodisperse building blocks is far more challenging for progressively larger structures.[16] Moreover, non-specific binding at larger scales results in a mixture of different structures rather than the desired product.[17] Nevertheless, at higher length scales, block-copolymers, and even molecular polymer brushes, have been reported to achieve structures with precise topography under controlled and narrow experimental conditions.[18,19]

Beyond molecular and supramolecular scales, nanoscale building blocks have enabled colloidal and supracolloidal self-assembly.[20] Specifically, noble metal nanoparticles (MNPs) have emerged as attractive building blocks for self-assembly and hierarchical structure formation.[21] The size and shape-dependent optoelectronic properties make noble metal nanoparticles and their self-assembled structures attractive for various applications, including catalysis, sensing, imaging, drug delivery, hydrogen evolution reactions, and photothermal therapy.[22] Furthermore, self-assembled superstructures allow nanoconfinement for selective encapsulation and can act as nanoflasks for chemical reactions.[23] Despite tremendous progress in plasmonic nanoparticle-based self-assembly, several challenges exist.[24] Importantly, the design of MNPs with well-defined shapes, sizes, and surface chemistry with precision still needs to be improved. Due to their high surface-to-volume ratio, MNPs have high surface energy. To minimize the surface energy, they undergo uncontrolled aggregation. Furthermore, MNPs display polydispersity and lack directional interactions.[25] Importantly, underlying driving forces and the role of the solvent and other environmental factors that control the nanoparticle interactions are not fully understood. The complexity of the inter-particle interactions and the lack of mechanistic insights are major challenges in achieving controlled self-assembly.[26] For example, van der Waals, electrostatic, and steric interactions play a crucial role in nanoparticle self-assembly. However, the exact contribution of these forces and their dependence on nanoparticle size, shape, and surface chemistry remain to be determined.[27] The high surface energy of MNPs also destabilizes certain structures, limiting access to self-assembled 1D or 2D layered structures in a template or template-free manner.[28] Due to their isotropic nature, the self-assembly of spherical MNPs and other colloidal particles often results in 3D structures. Achieving 1D or 2D structures requires anisotropic interactions between the neighboring nanoparticles.[29] The inhomogeneous distribution of surface charge allows electrical dipoles. This approach can be utilized to achieve the dipole-induced self-assembly of nanoparticles into 1D structures provided the inter-nanoparticle interaction strength exceeds the thermal fluctuation energy and Coulombic repulsion.[30] External fields such as magnetic and electrical fields, selective ligand exchange, DNA functionalization, and spatial and shear confinement approaches have been utilized to achieve MNP-based 1D and 2D structures.[29–31]

Computational simulations have been used to study the self-assembly pathway and intermediates of metal nanoparticles.[32] Specifically, molecular dynamics (MD), coarse-grained (CG), and Monte Carlo (MC) simulations have been employed. CG and all-atom MD simulations have been used to gain insights into the effects of ligand density on self-assembly and intermolecular forces at the nanoscale.[33] Recent studies using all-atom MD simulations have revealed that for gold nanoparticles (AuNPs) coated with dodecanethiol in a toluene-ethanol/water interface, self-assembly is dominated by interactions between the ligands, specifically van der Waals interactions.[34] Furthermore, self-assembly depends on the evaporation rate: slow evaporation results in two-dimensional (2D) arrays. Replacing dodecanethiol ligands with mercaptoundecanoic acid results in a roughly ordered, close-packed array with faster aggregation independent of the evaporation rate. This is attributed to the strong polarizing nature of mercaptoundecanoic acid molecules and the strong interactions between them.

Importantly, over the past two decades, size and shape-controlled syntheses have allowed a range of stable noble metal nanoparticles,[35] providing routes for 3D crystals,[36] 2D layered structures,[37] and elastic membranes.[38] More detailed theoretical insights and experimental approaches for MNP-based 1D, 2D, and 3D assemblies are beyond the scope of this article and have been discussed in several recent reviews.[30,31] Moreover, MNP-based structures have been considered inorganic protein mimics.[39] Metallic helical structures,[40] chiral superlattices,[41] and isomeric clusters,[42] have also been developed. However, even with narrow size dispersed metal nanoparticles, the batch-to-batch variations, and inhomogeneous ligand density lead to irreproducible mechanical properties, poor device performance, and inaccurate sensing.[43,44]

The progress in molecular engineering, nanomaterials, fabrication methods, and tools for atomic-level manipulation have contributed to the development of atomically precise manufacturing (APM) approaches.[45] The potential applications of APM towards molecular electronics devices, single electron

Nonappa

Nonappa is an Associate Professor in the Faculty of Engineering and Natural Sciences at Tampere University, Finland. He received his PhD from the Indian Institute of Science, Bangalore, India. He conducted his post-doctoral research at the University of Jyväskylä and Aalto University, Finland. His current research interests include precision nanomaterials, colloidal self-assembly, hydrogels, bio-based optical fibers, in vitro breast cancer models, and cryogenic transmission electron microscopy.

transistors, quantum computing, and nanoresonators have been demonstrated.[46] A sophisticated positional control approach produces complex 3D objects but with precision for only a few atoms.[47] Furthermore, super-resolution nanolithography and combinatorial patterning have been reported for precision assemblies.[48] Despite numerous efforts, large-scale structure formation with atomic-level precision has remained challenging.

In colloidal science, polymer microparticles with controlled size, shape, and surface functionalities have been viewed as ''big atoms'' as an analogy to atoms.[49] Furthermore, it has been shown that discrete clusters of colloidal microparticles can be achieved with a wide range of geometries.[50] The resulting finite clusters of colloidal particles are referred to as ''colloidal molecules'' as they mimic the symmetry of molecular structures.[51] The colloidal clusters sustain Brownian motion and allow real-time imaging. Therefore, they act as model systems to investigate the structure, dynamics, and self-assembly properties at the mesoscale. Block-*co*-polymers, such as triblock co-polymers, offer microparticles with rich surface chemistry, anisotropy, and patchiness.[52] Recent experimental studies and computational simulations have shown that patchy colloidal particles offer routes for designing new assemblies with emerging optical properties.[53–55]

Despite rapid increases in experimental studies and computational simulation in colloidal clusters and plasmonic nanoparticles, identifying the exact number of interacting units at atomic-level precision remains a major challenge. Resolving this issue by using ''strictly monodisperse'' nanoscale building blocks with engineered properties would represent a significant advance in nanoengineering. This would enable new assembly methods for low-cost, large-area, and flexible devices using solution processing methods to meet the ever-growing demand to integrate next-generation functional devices. In this context, precision nanoengineering, *i.e.*, engineering atomically precise nanoscale building blocks and developing methods for their fabrication into large-scale structures can overcome the challenges faced in manufacturing precision across length scale. Furthermore, the approach will bridge the gap between molecular and colloidal self-assemblies.

Precision nanoengineering has no formalized definition. However, in the context of this feature article, it encompasses the design, synthesis, and characterization of atomically precise nanoscale building blocks for the fabrication of materials, devices, and systems across length scales. The approach will provide routes for self-assembled discrete structures, composites, and large-scale defect-free structures. Due to the atomic-level precision of the building blocks, the position, orientation, and interaction of each unit can be specified. The fabrication may involve one, two, or more than two types of building blocks or components. When two or more building blocks are involved, at least one of the components is atomically precise, while the other is narrowly size dispersed ($<5\%$ dispersity). The components can be either synthetic (*e.g.*, atomically precise metal nanoparticles, organic nanoparticles, or organic–inorganic hybrids), biological nanoparticles (*e.g.*, proteins, virus particles, or DNA origamis), or narrowly size dispersed synthetic nanoparticles. Unlike APM, here, the focus is to utilize the atomically precise nanoparticle building blocks for higher-order structure formation. Since the building blocks are atomically precise and at the colloidal level, self-assembly will result in atomically precise higher-order structures. In this context, recent progress in the size and shape-controlled synthesis of monolayer thiol-protected atomically precise noble nanoclusters (NCs) provide new routes to realize precision nanoengineering-enabled self-assemblies across length scales.[56,57]

In the next section of this feature article, I will discuss the following: (i) the state-of-the-art challenges in the self-assembly of atomically precise NCs; (ii) how to obtain clues from biological colloidal molecules to achieve efficient and error-free self-assembly across length scales, *i.e.*, structures that span multiple size regimes, from the nanoscale to the macroscale; (iii) how to exploit the patchy and anisotropic distribution of ligands on the NC surface for self-assembled 2D colloidal crystals, macroscopic membranes, capsids, and composite cages; (iv) new methods for NC-based reversible frameworks using dynamic covalent chemistry; and (v) *in situ* synthesis and site-selective doping of photothermally stable NCs on colloidal templates. Specifically, the focus is on atomically precise gold (Au) and silver (Ag) NC-based self-assembled structures. Beyond structure formation, the goal is to design systems with specific properties and functions. Therefore, these self-assembled structures are referred to as functional self-assemblies. Accordingly, the self-assembly-induced amplification or emergence of photophysical properties, catalytic efficiency, and mechanical properties are discussed. The need for building blocks with atomic precision in controlled structure formation, reproducible optomechanical properties, and sensing is highlighted. The importance of self-assembly in the amplification of photoluminescence quantum yield, catalytic efficiency, bioimaging, sensing, and photothermal stability is also presented.

2. Atomically precise nanoclusters

To utilize any building block for controlled structure formation, well-defined structures, functional groups, directional interactions, and stability are needed. Atomically precise monolayer thiol-protected noble metal NCs with a few to hundreds of atoms have emerged as an important class of nanomaterials.[58] Despite more than six decades of history,[59,60] their extensive structural characterization, understanding of their optoelectronic properties, and applications of atomically precise nanoclusters have emerged only in the past two decades.[61–63] Because of their well-defined structure, various characterization tools are routinely used to determine the molecular structure, composition, and optical and electronic properties of NCs.[64] The molecular structure at atomic-level resolution is crucial for understanding the packing of metal atoms, the position and orientation of ligands, and molecular packing in macroscopic crystals. Single-crystal X-ray diffraction (SCXRD) is the most powerful method for complete structure determination.

However, X-ray diffraction requires pure and high-quality crystals of NCs. Due to their large size, obtaining single crystals suitable for diffraction is challenging. Despite these challenges, several reports have presented high-resolution single-crystal X-ray structures of NCs. Notably, in 2007, Jadzinsky *et al.* reported the first crystal structure of monolayer thiol-protected water-soluble Au NC, Au_{102}-*p*MBA_{44}.[65] In 2008, Zhu *et al.* reported the crystal structure of phenylethane thiol-capped, 25-atom gold cluster, $Au_{25}PET_{18}$.[66] Since then, more than 100 single-crystal X-ray structures of AuNCs, Ag NCs, and alloy NCs have been reported in the literature.[67] However, most of the crystal structures reported in the literature are for NCs soluble in organic solvents. The crystallization of water-soluble NCs is still a major challenge. Recently, cryogenic transmission electron microscopy (cryo-TEM) and single-particle reconstruction methods have been employed for atomic-level structure determination of water-soluble *m*-mercaptobenzoic acid (*m*MBA)-capped Au_{68} NC and *p*MBA-capped Au_{144} NC.[68] However, under cryo-TEM, only the metal core was unambiguously assigned, and identifying ligands is a challenging task. Therefore, other analytical tools with computational modeling were used to predict the number of ligands. In another approach, microcrystal electron diffraction (microED) has been used to determine the structure of Au_{146}-*p*MBA_{57} beyond 1.0 Å resolution.[69] Electrospray ionization mass spectrometry (ESI-MS), matrix-assisted laser desorption ionization (MALDI-MS), ion mobility coupled to mass spectrometry (IM-MS), and collision-induced dissociation (CID) MS techniques are extensively used to determine the molecular composition, to monitor the reaction kinetics, ligand exchange and ion exchange in NC synthesis.[70] One-dimensional (1D) and two-dimensional nuclear magnetic resonance (2D NMR) spectroscopy have been used to study the solution state stability of NCs, ligand composition, charge state, magnetic properties, and their dynamics.[71] X-ray absorption spectroscopy (XAS) has been used to determine the local structure and electronic state of a specific element within the NC, in both amorphous and crystalline solids.[72a] One of the important characterizations is their oxidation state, which can be determined by calculating the binding energy using X-ray photoelectron spectroscopy.[72b] Unlike plasmonic nanoparticles, due to the quantum confinement effect, NCs display molecule-like optical transitions in the absorption spectra. Based on the number of metal atoms, the UV-Vis absorption spectra of NCs show distinct absorption bands irrespective of the type of ligands.[73] Another important property of NCs is their photoluminescence (PL); therefore, photoluminescence spectroscopies, including steady-state, time-resolved, and temperature-dependent PL spectroscopies, have been used to study these properties,[73a] and to understand the correlations of the ultrafast electron dynamics and structures of NCs, such as femtosecond time-resolved fluorescence up-conversion, and transient absorption.[73c]

Because of their atomically precise structure and strictly defined number of ligands, NCs are considered ''colloidal molecules'' with hierarchical structural complexity.[74] It is important to clarify that the term ''colloidal molecules'' used in the literature for colloidal clusters is an analogy to molecular structure, and colloidal clusters do not have the properties of molecules. On the other hand, atomically precise NCs have strictly defined molecular structure, molecular mass, and optical properties despite their colloidal-level size. Therefore, NCs act as a link between organometallic complexes and large plasmonic nanoparticles (Fig. 1a and b). Beyond the atomically precise structure, NCs offer unique optical properties, tunable photoluminescence, photothermal stability, mechanical properties, biocompatibility, and low cytotoxicity (Fig. 1c–e).[75] Therefore, NCs offer numerous advanced applications, including catalysis, CO_2 reduction, bioimaging, solar concentrators, energy harvesting, photodynamic therapy, high harmonic generation, and dopants for field-effect transistors.[76–80] Precision nanoclusters are highly sensitive as compared to plasmonic nanoparticles for the addition or removal of metal atoms. This offers selective doping with amplified luminescence.[79] Therefore, a large library of molecularly precise nanoparticle-based building blocks can be prepared with unprecedented properties.

Atomically precise NCs have already played a significant role in biological imaging, providing high-resolution information on the location and orientation of subunits in oligomeric enzymes, virus capsids, crystalline sheets of membrane proteins, and thin filaments of muscle.[81] NCs are small and stable, making them ideal for labeling biological specimens for electron microscopy imaging. They are also highly versatile and can be used to label a wide variety of targets. For example, undecagold, the first commercial AuNC and the smallest immunogold, was first reported in 1969.[82,83] Since then, undecagold and other NCs have been extensively used for immunolabeling and high-resolution imaging of biological structures.[84] Excellent accounts of the historical perspectives, synthesis, characterization, optical properties, and applications can be found in several recent reviews.[57,58,85] As the field of NCs continues to develop, we can expect to see even more applications of these versatile NCs for new-generation functional materials. However, to achieve such targets, there is a need for focused research on developing approaches for the fabrication of NC-based structures and their integration into devices. Furthermore, NCs alone may not provide all the desired properties. Therefore, it is important to identify various combinations of materials and methods for NC-based composites and hybrid systems. In this context, self-assembly is one of the methods that can be used to achieve this, as it allows readily tunable morphologies.

2.1 State-of-the-art challenges in the self-assembly of atomically precise nanoclusters

Despite the exponentially increasing number of literature reports, the use of atomically precise NCs as a building block for self-assembly has been a recent trend.[86] Notably, Schmid *et al.* made early attempts to assemble phosphine-capped Au NCs on polymer-coated substrates.[87] Because of their small size and well-defined surface ligands, NCs have dispersion properties similar to supramolecular complexes.[88] Therefore, they are

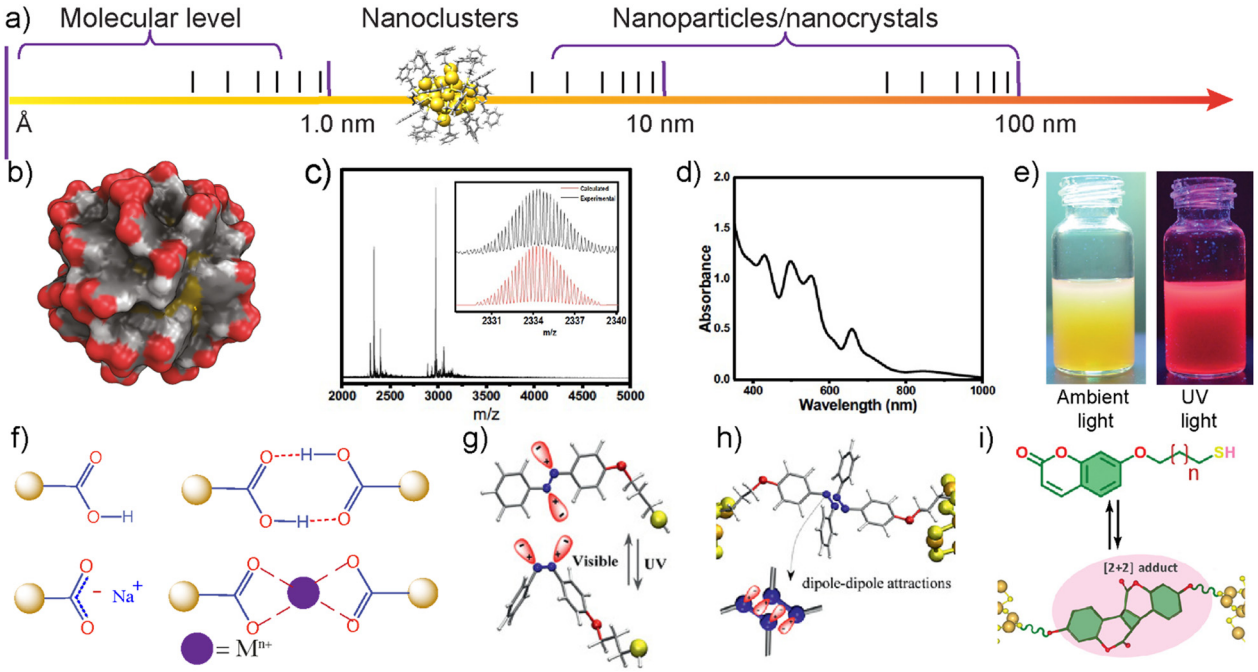

Fig. 1 The structure and properties of atomically precise gold and silver NCs. (a) Atomically precise NCs are bridging links between molecules, organometallic complexes, and large plasmonic nanoparticles. (b) Space-filling model showing the structure of Au_{102}-*p*MBA_{44} based on the crystal structure reported in ref. 60*a*. Reproduced with permission from ref. 110 Copyright © 2016 Wiley-VCH. (c) ESI-mass spectra of Na_4Ag_{44}-*p*MBA_{30}. (d) UV-Vis absorption spectra of Na_4Ag_{44}-*p*MBA_{30} showing molecule-like electronic peaks. Reproduced with permission from ref. 114 Copyright © 2022 Wiley-VCH. (e) Photographs of Au-BSA NCs showing luminescence. Reproduced with permission from ref. 145 Copyright © 2016 American Chemical Society. (f) Carboxylic acid groups on surface ligands allow hydrogen bonding, electrostatic repulsion, and metal chelation-induced assembly. (g) and (h) Dipole–dipole interactions of a thiolated azobenzene ligand using light-triggered isomerization. Reproduced with permission from ref. 141 Copyright © 2020 American Chemical Society. (i) Thiolated coumarin ligands allow dynamic covalent chemistry-assisted assembly *via* [2+2] photocycloaddition reactions. Reproduced with permission from ref. 143 Copyright © 2023 Wiley-VCH.

ideal building blocks for self-assemblies. Recent computational studies on experimentally determined gold nanoclusters have shed some light on their unique solubility properties.[89] However, their small size also poses significant challenges to achieving stable self-assembled structures in the solution. This is attributed to the fact that the inter-NC interactions are close to the thermal fluctuation energy of the surrounding media.[90] Therefore, access to large-scale structures using self-assembly in solution remained a challenge until recently.

According to the classical Derjaguin, Landau, Verwey and Overbeek (DLVO) theory, the stability of colloidal particles in a dispersion medium depends on the sum of attractive van der Waals interactions and electrostatic or steric repulsions.[91] The DLVO theory was initially formulated for two identical particles. It is based on the assumptions that (i) van der Waals attraction forces and electrostatic double layer forces are independent of each other, (ii) the two forces can be superimposed or added at each interacting distance for two particles, (iii) changes in the ionic strength control the range of the double layer interaction, and (iv) van der Waals forces are independent of ionic strength.[92] Therefore, the initial assumptions seriously limit the application of the classical DLVO theory for accurately studying colloidal stability. Several non-DLVO forces, including solvation, solvophobic, and charge correlation forces, were not considered in the original DLVO theory.[93] Therefore, several modified or extended DLVO theories have been proposed to study a wide range of colloidal forces.[94] Modified DLVO theories have been extended to metal nanoparticles, rod-like particles, and 2D nanomaterials.[95] This has contributed tremendously to understanding the self-assembly of polymer-based colloidal particles, metal nanoparticles, and hybrid colloidal assemblies. However, more attempts are needed to develop concepts for self-assemblies for atomically precise NCs.

3. Biological particles provide clues for the assembly of colloidal molecules

Traditional DLVO theory cannot be applied to biological systems such as virus capsid assembly. Short-range interactions and specific ion effects play a major role in biological systems.[96] Therefore, understanding how biological colloidal-level molecules such as virus capsids undergo assembly will provide crucial insight into the self-assembly of synthetic colloidal molecules. Because of their unique structure, virus capsids have been an intense topic of research and mathematical puzzle in the mid-20th century.[97–100] In 1950 H. R. Crane proposed a subassembly concept to describe the assembly process of the virus capsid.[99] This term *subassembly* was used as an analogy to the automobile factory assembly process at

that time. Subsequently, the concept of self-assembly has gained momentum. In 1956 Watson and Crick proposed that plant virus can be considered a *molecule* because of its high degree of order at atomic level resolution.[101] In 1969 an extended essay by Kushner detailed the sub-unit-based self-assembly of virus capsids.[102] Each subunit is atomically precise with a well-defined structure. In proteins, the partial double-bond character of peptide bonds imparts conformational rigidity to their primary structure. In their secondary structure, well-defined intramolecular interactions provide structural rigidity to the proteinic subunits.

The secondary structure of folded units displays patchy interacting sites, facilitating error-free tertiary structure formation. The patchy interactions are guided by hydrogen bonding, electrostatic repulsion, the hydrophobic effect, and specific interactions between Caspar pairs.[103] Each subunit has an interacting distance that is much smaller than a nanometre. Therefore, the self-assembly of nanoparticles below 3 nm can be achieved, provided there are structural and conformational rigidity, patchy interacting sites, and directional supramolecular interactions. Fig. 2a shows the protein subunits and hierarchical assembly of the cowpea chlorotic mottle virus (CCMV) based on the X-ray crystal structure.[104] It is important to note that the virus capsid self-assembly is highly complex due to numerous interactions, including nucleic acid (RNA or DNA)–protein interactions and metal chelation that stabilize the protein envelope.[104]

In molecular-level building blocks, conformationally rigid surfactants have been shown to display similar self-assembly patterns to that of peptides.[105] Importantly, the rigid surfactants and peptides are chemically dissimilar, still producing similar structures. Similarly, identifying the structural features in nanoparticle building blocks that mimic virus capsid proteins and capsids may offer routes for precision structures other than routinely observed 3D crystals. Furthermore, tuning the experimental conditions may result in a diverse set of

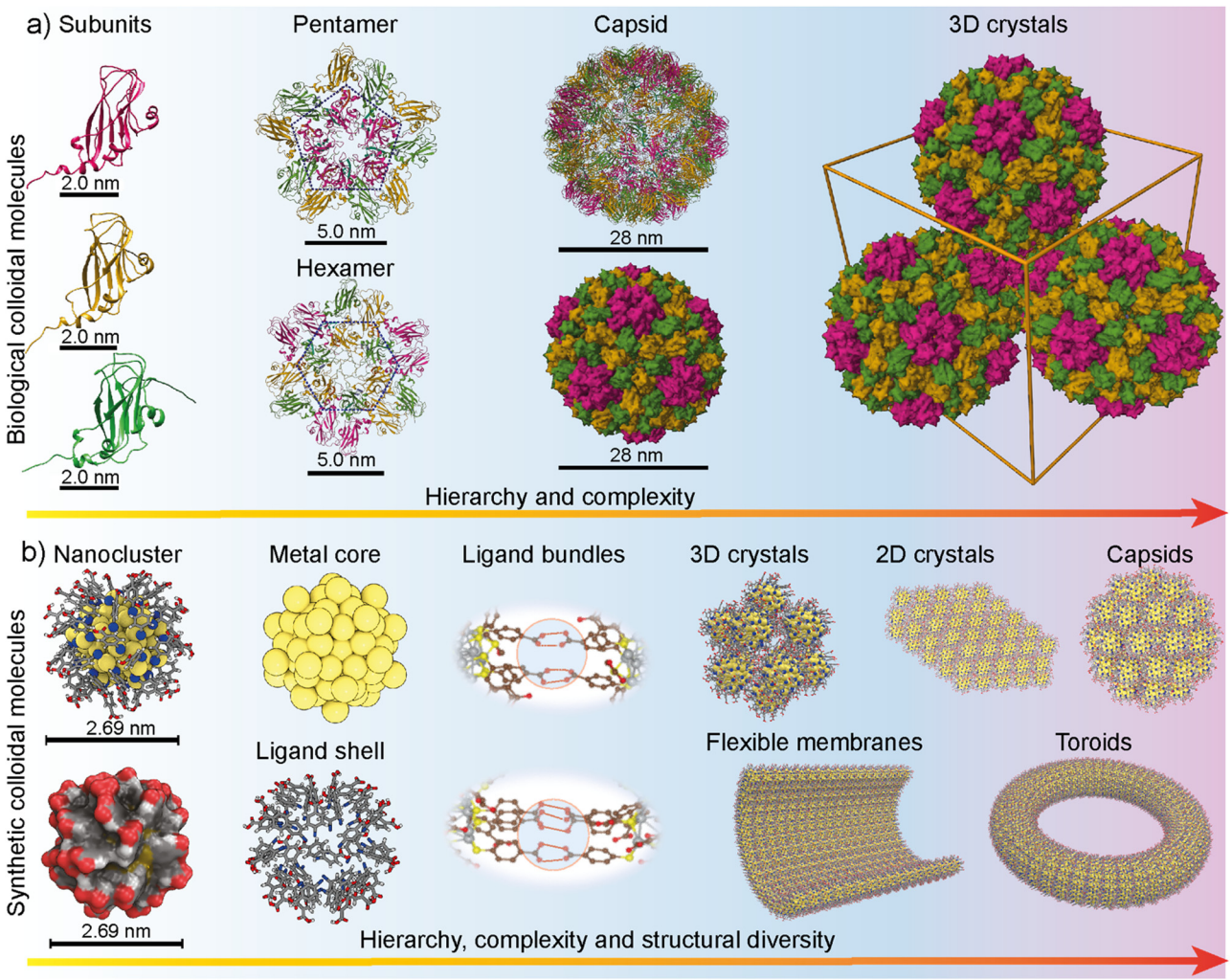

Fig. 2 Atomically precise colloidal molecules. (a) Subunit-based self-assembly of the cowpea chlorotic mosaic virus (CCMV) with increasing complexity driven by patchy interactions of subunits based on the crystal structure (PDB ID: 1CWP) reported in ref. 104. (b) Metal nanoclusters display rigid core and monolayer ligand shells, patchy ligand bundles and allow hierarchical self-assembly and structural diversity. Reproduced with permission from ref. 86 Copyright © 2018 Wiley-VCH.

morphologically distinct structures (Fig. 2b). Therefore, utilizing atomically precise metal nanoparticle-based self-assembly concepts offers precision nanoengineering under a broad range of experimental conditions, including temperature, pH, light, and solvent parameters. Importantly, virus capsid proteins and designer DNA-origamis have been used to hybrid superlattices with plasmonic nanoparticles with unique packing patterns, morphology, and optical properties.[106] However, such structures are delicate and are obtained only under very narrow or specific experimental conditions.

4. Patchy ligand distribution and symmetry breaking

X-ray crystal structures of monolayer thiol-protected Au and Ag NCs revealed some of the salient features of the NCs (Fig. 2b and 3). Importantly, (i) the metal atoms form the intrinsically rigid core, (ii) ligands are covalently linked to the metal atoms and often present in bundles, (iii) ligands (specifically aromatic ligands) display conformational rigidity due to inter-ligand interactions and orientation, and (iv) ligand bundles result in patchy and anisotropic distribution of interacting sites (Fig. 3b–d). Therefore, NCs have some similarity to the virus capsid subunits in their size, structural features, and patchy interacting sites. These properties can therefore be exploited to fabricate higher-order structures by tuning the experimental conditions and promoting selective interaction between the patchy interacting sites.

Jadzinsky *et al.* reported the single-crystal X-ray structure of *p*-mercaptobenzoic acid (*p*MBA)-capped AuNC, Au_{102}-*p*MBA_{44}.[65] The NCs undergo crystallization in acetic acid/methanol solvent mixture.[107] More importantly, when the carboxylic acid groups of all ligands are in the protonated form, Au_{102}-*p*MBA_{44} is dispersible in methanol but insoluble in water. However, for partial deprotonation, *i.e.*, when ~50% of the carboxylic acid groups are deprotonated, the NC is water-dispersible but insoluble in methanol. An extensive nuclear magnetic resonance spectroscopy study has revealed that the *p*MBA ligands in NC are chemically and magnetically non-equivalent.[108] Consequently, the deprotonation is not random but results in patchy negative charges due to slight differences in the pK_a values of the carboxylic acid groups.[109] The patchy and negatively charged surface also imparts amphiphilic properties to the NC.

4.1 2D colloidal crystals and monolayer membranes

Nonappa *et al.* demonstrated the self-assembly of Au_{102}-*p*MBA_{44} NC in aqueous media (Fig. 4a–c).[110] A systematic investigation of the solid-state structure using a spherical coordinate system revealed the patchy distribution of the ligands on the nanoparticle surface (Fig. 3b and c). The ligands were anisotropically distributed with a preferential arrangement around the equatorial plane (Fig. 3d). The anisotropic and patchy distribution allows symmetry breaking, offering routes for lower dimensional structures. This was achieved using a dispersion of Au_{102}-*p*MBA_{44} in aqueous NaOH, which led to a highly stable dispersion with a zeta potential of −69 mV. When the aqueous

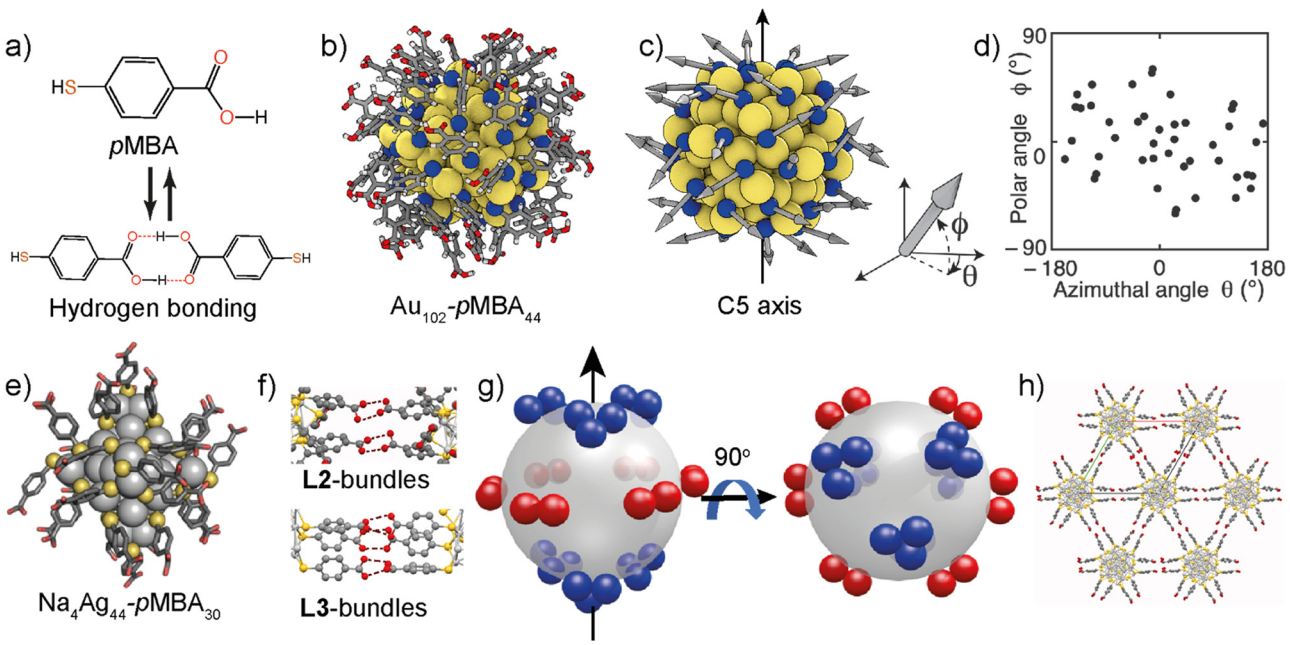

Fig. 3 Anisotropic and patchy ligand distribution. (a) Chemical structure of the *p*-mercaptobenzoic acid (*p*MBA) ligand and hydrogen bonding dimerization. (b) Crystal structure of Au_{102}-*p*MBA_{44}; yellow (Au), blue (S), black (C), red (O), and white (H). (c) and (d) The ligands are indicated with arrows to determine their position, orientation, and location using a spherical coordinate system. (d) The ligands are anisotropically and preferentially distributed around the equatorial plane of an imaginary axis. Reproduced with permission from ref. 110 Copyright © 2016 Wiley-VCH. (e) The crystal structure of Na_4Ag_{44}-*p*MBA_{30}. (f) Hydrogen bonding ligand bundles in Na_4Ag_{44}-*p*MBA_{30}. (g) Schematic representation showing the distribution of L2 bundles around the equatorial plane and (h) by preventing interlayer interaction and promoting intralayer hydrogen bonding, 2D structures can be realized. Reproduced with permission from ref. 114 Copyright © 2022 Wiley-VCH.

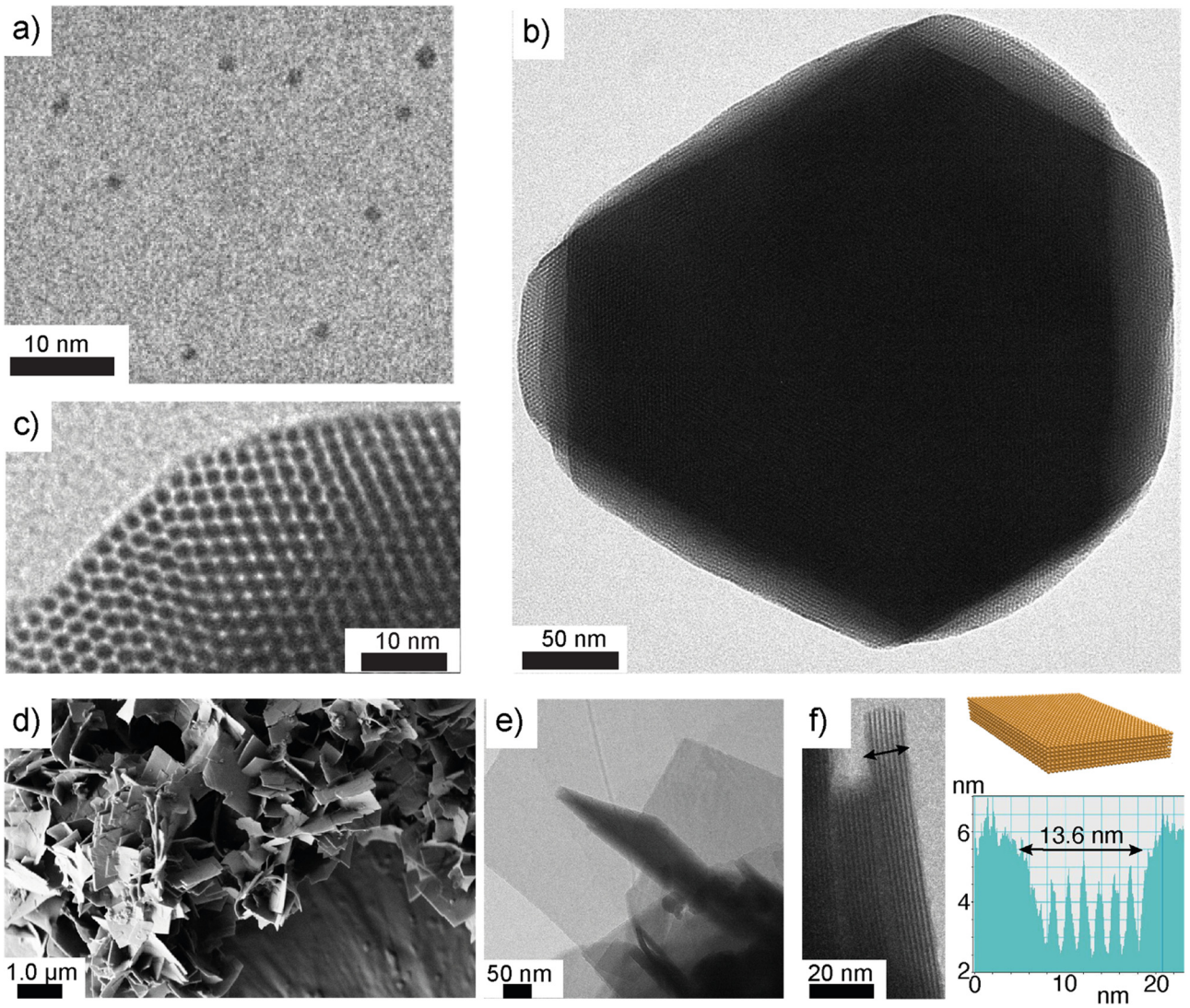

Fig. 4 NC-based 2D colloidal crystals. (a) TEM image of Au_{102}-*p*MBA_{44} NCs. (b) TEM image of a self-assembled 2D colloidal crystal. (c) TEM image from a selected monolayer showing hexagonally close-packed NCs. Reproduced with permission from ref. 110 Copyright © 2016 Wiley-VCH. (d) SEM image of self-assembled 2D colloidal crystals of Na_4Ag_{44}-*p*MBA_{30} NC in methanol. (e) and (f) TEM images of self-assembled 2D colloidal crystals suggest that the thickness of each layer is close to the diameter of individual NCs. Reproduced with permission from ref. 114 Copyright © 2022 Wiley-VCH.

solution was sequentially solvent exchanged to methanol *via* controlled dialysis, 2D crystals were formed (Fig. 4a–c).

The partial deprotonation of the carboxylic acid groups allows a delicate balance between electrostatic repulsion and attractive hydrogen bonding interactions. The electrostatic repulsion prevents uncontrolled aggregation and random structure formation. The carboxylic acid dimerization promotes inter-NC interaction. The 2D colloidal crystals were comprised of a few layers with hexagonal close packing of NCs. Notably, the thickness of each layer corresponds to the diameter of one NC (Fig. 4b and c). This study provided the first evidence that low-dimensional structures can be achieved using solution-state self-assembly of atomically precise gold NCs. However, there are certain limitations to this approach. For example, continued dialysis resulted in further aggregates. Additionally, some heterogeneous populations were observed. Therefore, to achieve large-scale structures, improved methods and concepts are needed.

Desireddy *et al.* reported the synthesis and characterization of *p*MBA-capped AgNC, Na_4Ag_{44}-*p*MBA_{30} (Fig. 3e).[111] The ultra-stable nature and unique packing patterns in its solids state make this NC an attractive building block for self-assemblies.[112] Na_4Ag_{44}-*p*MBA_{30} forms rhombohedral crystals with the R3C space group. The NCs are hexagonally arranged *via* inter-NC hydrogen bonding. Unlike Au_{102}-*p*MBA_{44} NC, patchy ligand bundles are distinct in Na_4Ag_{44}-*p*MBA_{30}. The crystal structure has layered structures with two types of ligand bundles, *viz.*, bundles of two, **L2**, and bundles of three, **L3** (Fig. 3f). There are six **L2** bundles and six **L3** bundles. The **L2** bundles promote intra-layer hydrogen bonding (Fig. 3f). In contrast, the **L3** bundles promote interlayer hydrogen bonding. More importantly, all six **L2** bundles are positioned in the equatorial plane.

Therefore, each nanocluster forms 24 intralayer H-bonds using **L2** bundles (Fig. 3g and h). On the other hand, **L3** bundles are distributed in two patches, three at the top and three at the bottom of an imaginary axis. Therefore, they contribute 18 hydrogen bonds each. This leads to a greater number of hydrogen bonds in the equatorial plane. Som *et al.* utilized Na_4Ag_{44}-*p*MBA_{30} to prepare crossed-bilayer structures of tellurium nanowires by exploiting the preferential interaction between **L3** bundles.[113]

Recently, Som *et al.* demonstrated the preparation of strong and elastic large-area monolayer membranes of Na_4Ag_{44}-*p*MBA_{30} NC.[114] Due to the unstable nature of the Na_4Ag_{44}-*p*MBA_{30} in aqueous media, the self-assembly approach used for Au_{102}-*p*-MBA_{44} NC was not feasible. Therefore, the dispersion of Na_4Ag_{44}-*p*MBA_{30} in *N*,*N*-dimethyl formamide (DMF) was first tested for self-assembly in alcohols. In all tested lower alcohols (methanol, *n*-propanol, and *n*-butanol), a few layered 2D colloidal crystals were formed (Fig. 4d–f). The thickness of each layer corresponds to the size of one nanoparticle. In the next approach, the unique ability of 1-pentanol to form a transient layer when added to an aqueous surface was exploited. For this approach, the NCs were sequentially exchanged by precipitation and redispersion from DMF to 1-pentanol. The dispersion of Na_4Ag_{44}-*p*MBA_{30} in 1-pentanol was added dropwise onto the surface of water in a container. This resulted in a transient layer of 1-pentanol in which Na_4Ag_{44}-*p*MBA_{30} NCs were trapped. Due to the predominant intra-layer hydrogen bonding, the NCs encapsulated in the transient layer furnished a stable film (Fig. 5a). This allowed a macroscopic monolayer membrane that could be readily transferred to different substrates without any surface pre-treatment (Fig. 5b). Using UV-vis and Raman spectroscopy, it was shown that the monolayer membranes retained the characteristics peaks of individual Na_4Ag_{44}-*p*MBA_{30} NCs.

However, due to possible electronic coupling between the NCs in membranes, the absorption peaks were slightly broader as compared to that of individual NCs. The TEM imaging of the monolayer film displayed regular hexagonal packing of NCs with a periodicity of 2.01 nm and inter-NC distance of 2.23 nm (Fig. 5c–f). The self-standing nature of the membranes was supported using TEM and atomic force microscopy (AFM) imaging of the membranes placed over a TEM grid with a holey carbon support film (Fig. 5g–i). The AFM-based force spectroscopy revealed that the membranes are strong and elastic with Young's modulus values between 10 and 30 GPa with Gaussian distribution centred at 14.5 ± 0.2 GPa (Fig. 5j–l). Importantly, Young's modulus values of NC membranes displayed a narrow distribution. Notably, the observed Young's modulus values were much higher than plasmonic nanoparticle-based membranes prepared using highly sophisticated DNA nanotechnology.[34e] Plasmonic gold nanoparticle membranes reported in the literature showed highly scattered Young's modulus values.[38b] This suggests the importance of atomically precise building blocks with well-defined inter-particle interactions for high mechanical strength and reproducible mechanical properties.

Precision NC-based monolayer membranes offer ultrasmall nanogaps. Such systems can generate very strong and tunable electromagnetic fields for obtaining strong surface-enhanced Raman scattering (SERS) signals from Raman dyes.[115] It was shown that Na_4Ag_{44}-*p*MBA_{30} membranes could detect Raman-active antibiotic molecules such as amphotericin B at a concentration as low as 2.5 μg mL^{-1}. However, when identical experiments were performed using polydisperse Ag nanoparticles, the characteristic peak of amphotericin B was not observed at low concentrations. More importantly, the NC membranes showed highly reproducible SERS signals suggesting the importance of atomic precision in reliable and reproducible sensing.

4.2 Supracolloidal capsids and frameworks

Spherical superstructures using plasmonic nanoparticles are well documented in the literature.[23,116] Unlike plasmonic nanoparticles, the presence of directionality in NCs allows high control over their size, shape, and shell thickness. Nonappa *et al.* demonstrated the self-assembly of Au_{102}-*p*MBA_{44} into spherical colloidal capsids with monolayer shells (Fig. 6a–g).[110] This was achieved by adding the aqueous dispersion of partially deprotonated Au_{102}-*p*MBA_{44} NCs to methanol instead of controlled dialysis. In dialysis, hydrogen bonding dimerization between the protonated carboxylic acid groups provides attractive interactions. The partially deprotonated negatively charged carboxylates facilitate electrostatic repulsion. Therefore, the presence of both attractive and repulsive interactions can overcome the irreversible aggregation, leading to hexagonally packed 2D crystals. On the other hand, methanol is a non-solvent for partially deprotonated Au_{102}-*p*MBA_{44} NCs. Therefore, the rapid addition of aqueous dispersions to methanol may result in aggregation and defect-induced curvature formation furnishing spherical superstructures.[90,110] Apart from spherical superstructures, ellipsoidal capsids were also observed (Fig. 6e). Importantly, the inter-capsid hydrogen bonding facilitated by an ensemble of nanoclusters led to dimeric, trimeric or higher order structures (Fig. 6f and g). This suggests that the capsids with rich surface functionalities offer hierarchical structure formation with well-defined inter-capsid distance and order. More importantly, atomically precise NCs and narrowly size dispersed nanoparticles behave differently in their structure formation. For example, *p*-aminobenzoic acid-capped cobalt nanoparticles also formed capsids but with multilayered shells.[117,118] Due to the polydisperse nature of the nanoparticles, there was no regular order or arrangement of nanoparticles in the shell.

Bioimaging is one of the important applications of luminescent nanomaterials.[119] They offer rapid, low-cost, and sensitive imaging of cells with high spatial resolution. Routinely used fluorescent dyes such as rhodamine 6G show ultrabright fluorescence and high quantum yield. However, they undergo photobleaching, have the tendency to drop out of the cytoplasm, and are cytotoxic.[120] Photothermal stability, high quantum yield, bright photoluminescence, and large Stokes shifts are some of the key properties of nanomaterials for bioimaging. Despite the high quantum yield and photothermal stability, semiconductor quantum dots are intrinsically cytotoxic and undergo oxidation, preventing them from extensive use in biological applications.[121] Importantly, it has been demonstrated that

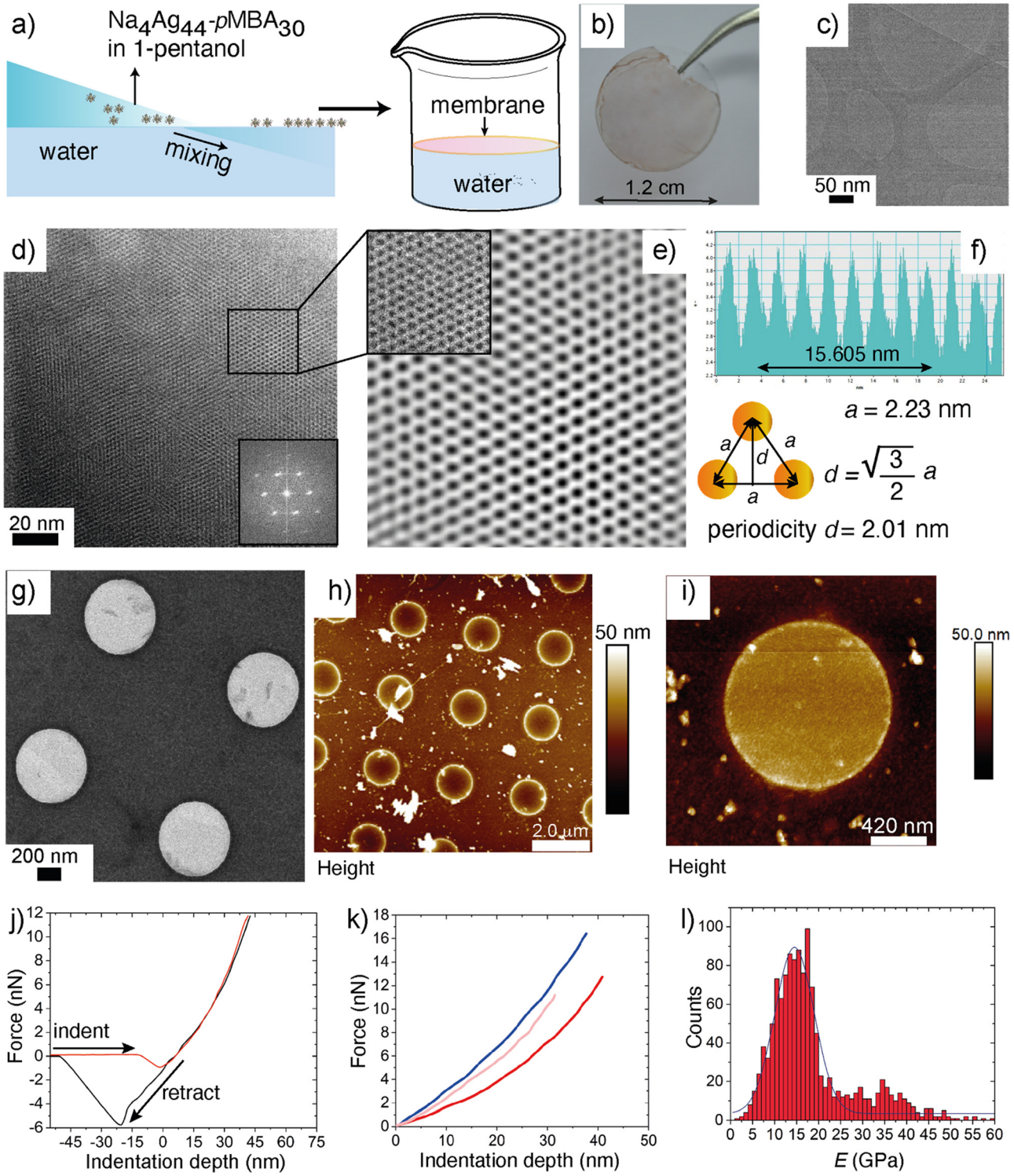

Fig. 5 Free-standing macroscopic monolayer NC membranes. (a) Schematics showing the transient solvent layer-mediated Na_4Ag_{44}-pMBA$_{30}$ NC. (b) Photograph of a large area of self-assembled Na_4Ag_{44}-pMBA$_{30}$ NC membrane on a cover slip. (c) TEM image of the Na_4Ag_{44}-pMBA$_{30}$ membrane stretched over a TEM grid with lacey carbon support film. (d) TEM image suggesting the hexagonal packing of Na_4Ag_{44}-pMBA$_{30}$ NCs (inset shows the FFT). (e) IFFT image from the marked area in image c. (f) Profile showing the inter-nanoparticle distance and periodicity. (g) TEM images of the monolayer membrane stretched over a TEM grid with holey carbon support film. (h) and (i) AFM images of the membrane. (j) A typical force-displacement curve suggesting the elastic nature of the membrane. (k) Overlap of $F(\delta)$ curves recorded on three different holes covered with membranes. (l) Histogram showing the Young's modulus (E) values extracted by fitting the $F(\delta)$ curves. Reproduced with permission from ref. 114 Copyright © 2016 Wiley-VCH.

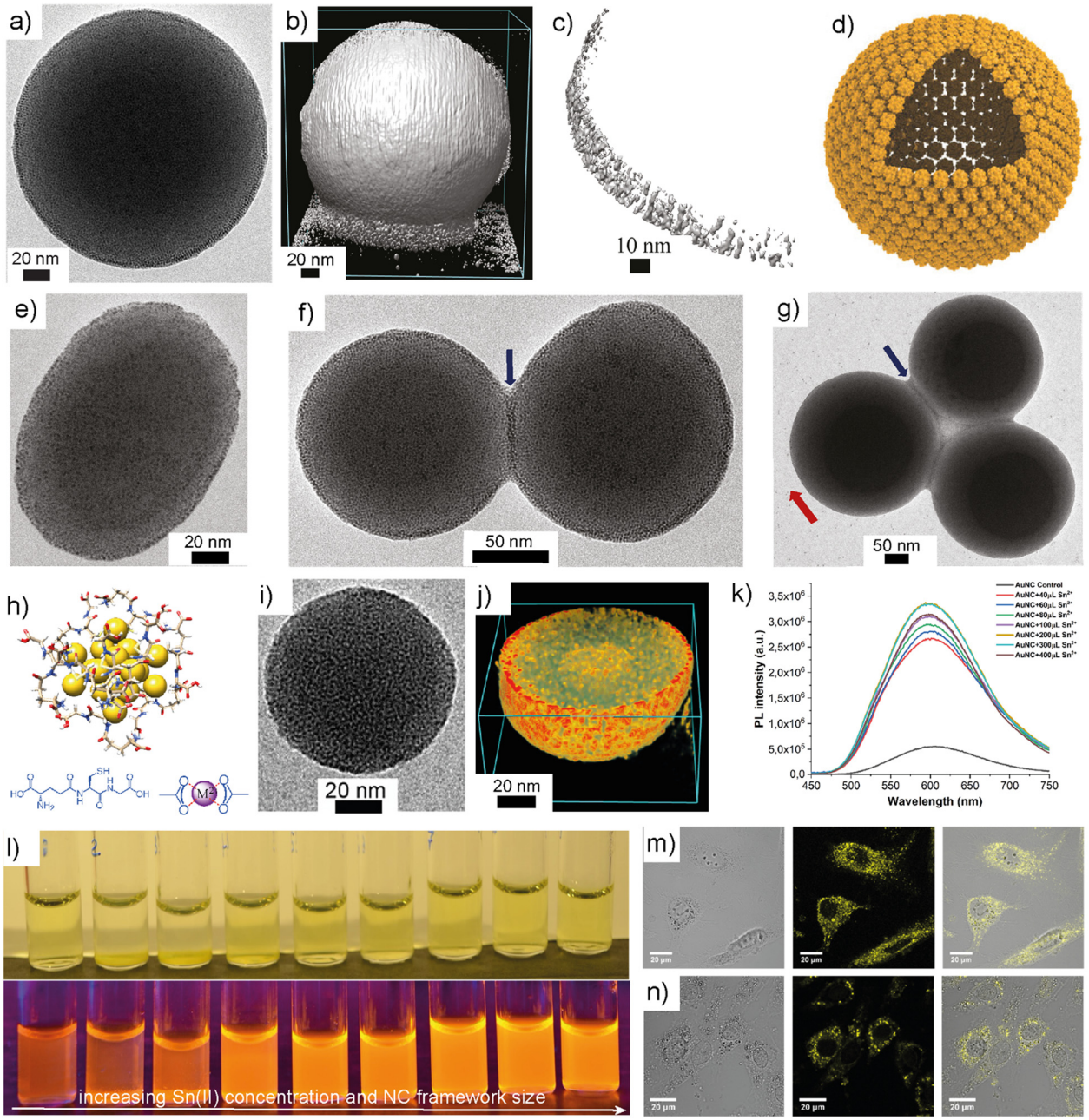

Fig. 6 Self-assembled capsids and frameworks. (a) TEM image of a TEM image of self-assembled Au_{102}-*p*MBA_{44} capsid. (b)–(d) TEM tomography, a cross-sectional view and schematic representation of a capsid with monolayer shell. (e)–(g) TEM images of ellipsoidal capsid, dimeric and trimeric structures showing inter-capsid bonding. Reproduced with permission from ref. 110 Copyright © 2016 Wiley-VCH. (h) Structure of glutathione capped gold NC. (i) TEM images of metal chelation-induced NC framework. (j) Electron tomographic reconstruction showing a cross-sectional view of NC frameworks. (k) and (l) The PL spectra and photographs of NC frameworks as a function of Sn(II) concentration. (m) and (n) Confocal microscopy images of NIH3T3 cells treated with NC frameworks. Bright-field image (left), confocal fluorescence image (middle), and overlapped image (right). Reproduced with permission from ref. 130 Copyright © 2019 Wiley-VCH.

the size and shape of nanoparticles have a significant effect on cell viability and cytotoxicity.[122] In this context, luminescent AuNCs have emerged as attractive nanomaterials for biomedical applications and multimodal imaging. The luminescence properties of Au(I) complexes containing phosphine and thiolate ligands are well documented in the literature.[123] The origin of such luminescence is due to strong ligand-to-metal charge transfer (LMCT) and ligand-to-metal-to-metal charge transfer (LMMCT).[124] In thiolate complexes, the origin of LMCT is attributed to S–Au(I) interactions, whereas the LMMCT is attributed to the attractive Au(I)···Au(I) interactions.[125] The attractive Au(I)···Au(I) interactions are referred to as aurophilic interactions, typically observed when the distance between adjacent Au atoms is below 3.6 Å. An extensive study by Cha *et al.* revealed that the Au(I)-alkanethiolate

complexes form highly ordered structures, and the luminescence properties depend on the electron-donating ability of thiolate ligands.[126] Furthermore, when the Au(I)-alkanethiolate complexes were used as precursors for nanoparticles in the presence of surfactants, the resulting nanoparticles showed no luminescence either in the solid or solution state. This raises the question of whether the luminescence observed in NCs is due to thiolate complexes or the NCs. Unlike plasmonic nanoparticles, in AuNCs, the presence of Au(0) core and Au(I)–S staple units on the surface contribute to the short bonding distances that affects their photoluminescent properties.[127] Extensive studies have been performed to understand the size-dependent luminescence properties, the effect of ligands, and aggregation-induced emissions.[128] However, the NCs suffer from low efficiency and quantum yield, and the luminescence is restricted to a certain type of NCs with specific ligands and composition. Importantly, the self-assembly of NCs can improve luminescence, stability, and quantum yield.[129] For example, metal coordination of functional groups on NC surfaces can rigidify the ligands and restrict their conformational freedom or mobility. This, in turn, amplifies the luminescence and photoluminescent quantum yield of luminescent NCs.

Chandra *et al.* demonstrated that water-soluble glutathione-capped AuNCs could be assembled into highly luminescent 3D spherical frameworks using metal coordination (Fig. 6h–j).[130] Specifically, the 3D frameworks were formed when the NCs interacted with $SnCl_2$. The metal chelation results in the reduction in non-emissive relaxation pathways. The quantum yield was increased from 3.5% for NCs to 25% in NC frameworks. By controlling the metal salt concentration, the size of the framework was tuned from 50 to 200 nm and consequently, the luminescence (Fig. 6k and l). UV-Vis and photoluminescence excitation spectra revealed that the frameworks retained the intrinsic properties of individual NCs. This suggests that the metal chelation-induced assembly is not a random aggregation. The results indicate that the framework formation is predominantly through metallosupramolecular interactions between the surface ligands and metal ions.

When the cell viabilities of NCs and NC frameworks were investigated in NIH3T3 and A549 cell lines, no significant cytotoxicity was observed (Fig. 6m and n). Importantly, in some cases, the viability was higher for frameworks and was pronounced when higher concentrations were used. This was attributed to the fact that NCs result in the generation of reactive oxygen species and the possible aggregation of NCs in the cellular medium before uptake leading to cell death. The bioimaging experiment revealed that the particles were in the cytoplasm and emitted brilliant fluorescent light when excited at 458 nm. Frameworks showed brighter emission than that of the NCs and thus the cells were easier to image. Beyond the amplification of PL, the NC frameworks also displayed improved photocatalytic activity under UV and visible light. The NC frameworks showed a 20-to-25-fold increase in their photocatalytic activity compared to that of NCs when a dye degradation experiment of methylene blue was performed under UV irradiation at 350 nm. Because of their well-defined 3D structures, the NC frameworks demonstrated enhanced adsorption of the dye molecules on their surface and interior, thereby, efficient catalytic activity. Therefore, the self-assembly of NCs not only offers tunable structures but also controllable optical properties, catalysis, biological activity, and imaging.

4.3 Nanoparticle-nanocluster composites

Anisotropic gold nanoparticles such as gold nanorods (AuNRs) display unique surface plasmon resonance peaks and high sensitivity to surrounding chemical environments.[131] AuNRs are known for their strong absorption and scattering in the near-infrared (NIR) region. Most human tissues, intrinsic chromophores, haemoglobin, and water have poor absorbance in the NIR region. Therefore, gold nanorods are efficient nanoprobes for *in vivo* imaging, targeted delivery, and photodynamic therapy.[132] Multimodal probes with synergistic properties can be achieved by integrating AuNRs with NCs in a single nanostructure. For example, interacting the AuNRs with organic dye molecules or quantum dots allows unique plasmon-exciton coupling.[133] Such interactions can be used to alter optical properties and signal amplification in plasmonic devices.[134]

Because of their molecule-like multiband electronic spectra and surface functionalities, NCs offer a unique opportunity to achieve plasmonic nanoparticle-NC interaction *via* supramolecular interactions between surface ligands.

Chakraborty *et al.* demonstrated the hydrogen bonding-directed encapsulation of plasmonic nanorods inside a nanocluster cage.[135] The gold nanorods ($d \approx 10$ nm, $l \approx 30$ nm) capped with *p*MBA ligands were treated with Na_4Ag_{44}-*p*MBA_{30} in DMF (Fig. 7). The presence of *p*MBA on the AuNR surface allows nanoparticle-NC interaction *via* hydrogen bonding. It was shown that the resulting nanorod-NC composite displayed peaks arising from the nanorod and NCs in their UV-vis spectra. This suggests that the intrinsic properties of both components were retained. However, due to possible electronic interactions between AuNR and NCs in the composites, significant broadening was observed in the NIR region of the spectrum. Using transmission and scanning transmission electron tomographic reconstruction, it was shown that the AuNR-NC co-assembly resulted in an octahedral cage (Fig. 7f and g). Notably, each cage encapsulated a single nanorod, offering a rapid and robust approach to composite supracolloidal cages. The selective encapsulation of nanoparticles was reported using highly sophisticated DNA nanotechnology with predefined size-specific structures with complementary base-pairing. Moreover, DNA nanotechnology has limitations as it requires cages and nanoparticles of precisely defined sizes. However, the self-assembly approach presented using NCs is independent of the nanorod or type of nanoparticles. The structures demonstrate the interaction of precision NCs with plasmonic nanorods with distinct optoelectronic properties. One would expect an amplification of certain properties or the evolution of new behaviour depending on the ligand length, core size, and inter-nanoparticle distance. The interactions can be controlled by modifying the functional groups of the ligands. For example, *p*MBA-capped AuNCs Au_{102}-*p*MBA_{44} and Au_{250}-*p*MBA_n interacted

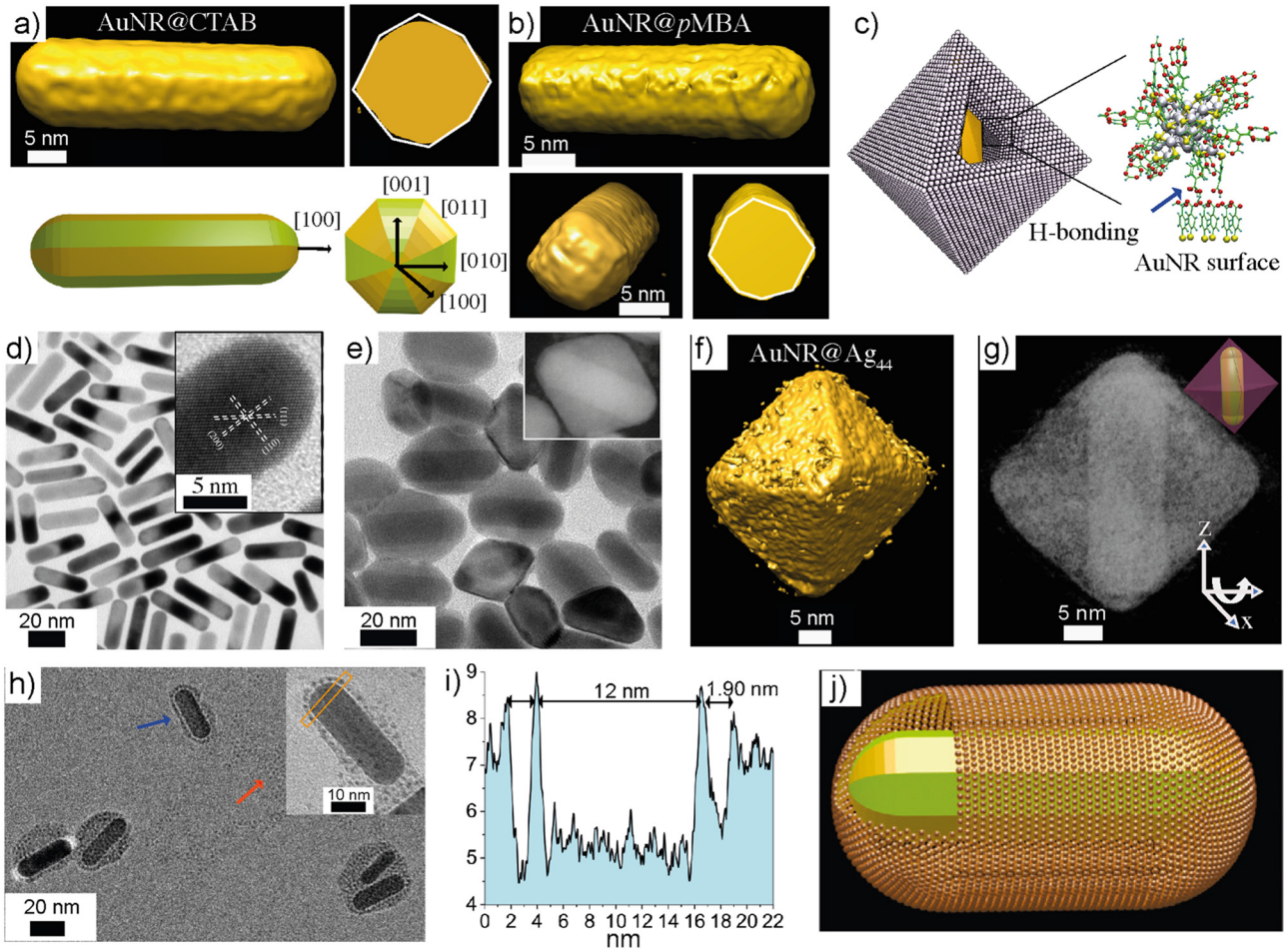

Fig. 7 Gold nanorod-NC composite cages. (a) and (b) Electron tomography of gold nanorods before and after ligand exchange. (c) Schematics showing the composite cage structure and nanorod-NC interaction *via* hydrogen bonding. (d) TEM image of *p*MBA-capped gold nanorods. (e) TEM image of composite cages (inset shows a DF-STEM image of a single composite cage). (f) and (g) Electron tomogram showing the isosurface and coloured views of a cage with nanorod orientation. (h) Gold nanorods, when interacting with water-soluble Au_{102}-*p*MBA_{44} showed monolayer shells around the nanorod. (i) The profile indicating the thickness of the shell. (j) A schematic representation of a composite cage with a monolayer shell. Reproduced with permission from ref. 135 Copyright © 2018 Wiley-VCH.

with *p*MBA-capped AuNRs in aqueous media. Unlike Na_4Ag_{44}-*p*MBA_{30}, the AuNCs produced a monolayer shell around the AuNRs (Fig. 7h–j). This is due to the negatively charged carboxylates on the NC surface, which provided sufficient electrostatic repulsion to stabilize the composite structures. Therefore, by controlling the ligand functional groups and reaction media, the shell thickness and the morphological features of the composites can be tuned.

In a recent study, Chakraborty *et al.* demonstrated the structural, morphological, and compositional diversity of nanoparticle-NC composites.[136] Specifically, gold nanotriangles (AuNTs) interacted with AgNCs with different ligand functionalities such as hexadecyltrimethylammonium chloride (CTAC), dimethyl benzenethiol (DMBT), and 1,2-bis(diphenylphosphino)ethane (DPPE). It was shown that depending on the type of ligand on the NCs, distinct composite structures and compositions were obtained when the NCs were reacted with CTAC-capped AuNTs. For example, the reaction between $Ag_{25}(DMBT)_{18}$ resulted in the etching of gold atoms from the tips of triangles and Ag-doped AuNTs. On the other hand, when the reaction was performed with $Ag_{25}H_{22}(DPPE)_8$, irregular dendritic shells of Ag were formed around the nanotriangle. Interestingly, faster gold etching was observed when Na_4Ag_{44}-*p*MBA_{30} was reacted with CTAC-capped AuNTs. Notably, when the AuNT surface was ligand exchanged with *p*MBA and interacted with Na_4Ag_{44}-*p*MBA_{30} NCs, a core–shell composite structure was formed (Fig. 8a and b). This suggests that directional hydrogen bonding prevents atom exchange or etching, resulting in a stable composite core–shell structure.

Plasmonic nanoparticles and nanoclusters are intrinsically sensitive to high-energy electron beams. Furthermore, when directional interactions are not possible, mixing two types of nanoparticles may lead to atom exchange or alloy formation.[137,138] Atom transfer and unwanted side reactions can be prevented by growing a protective layer around nanorods with substrates such as silica. The silica coating over nanoparticles provides anchoring for NCs and improves the photothermal stability of nanoparticles. Furthermore, the coating layer between nanorods and NCs also

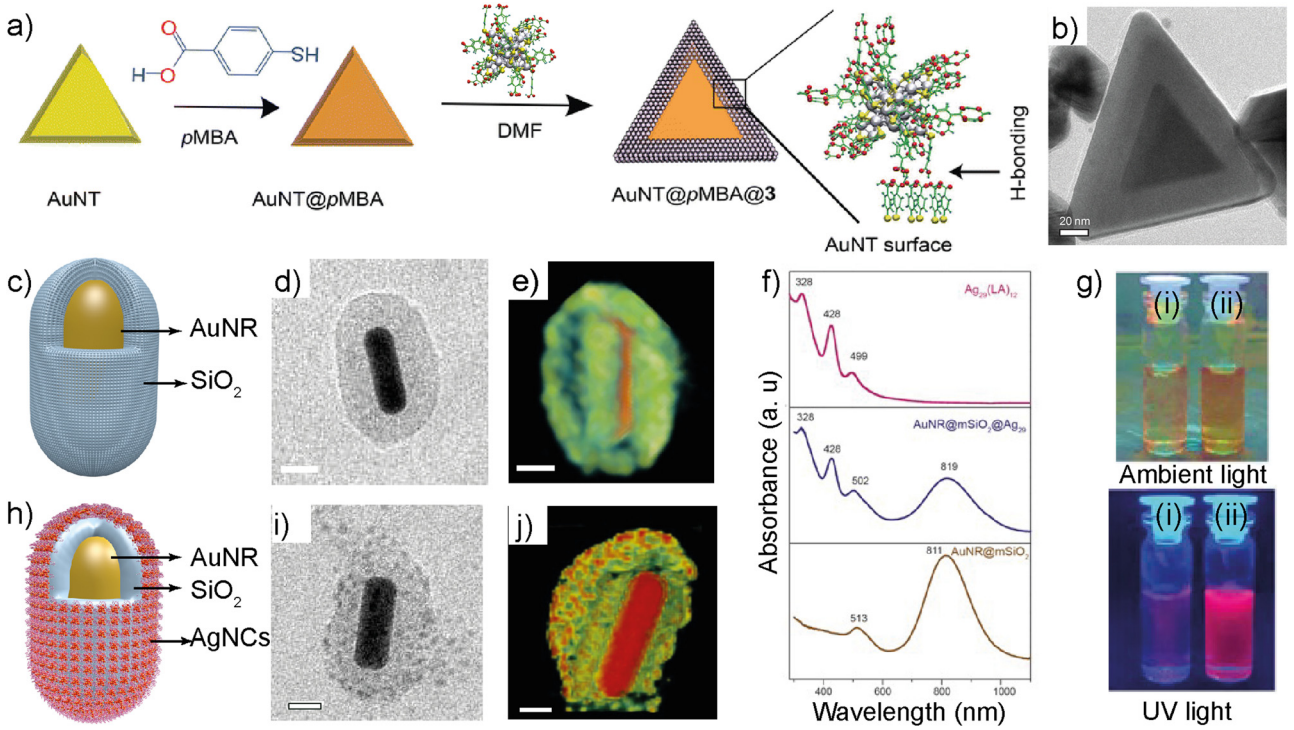

Fig. 8 Effect of ligand chemical structure and interaction on nanoparticle-NC reaction. (a) Shows a schematic representation of a gold nanotriangle (AuNT), ligand exchange, and core–shell structure formation. (b) TEM image showing a core–shell composite of *p*MBA-coated AuNT and Na_4Ag_{44}-*p*MBA_{30}. Reproduced with permission from ref. 136 Copyright © 2023 Royal Society of Chemistry. (c) Schematic representation of silica-coated gold nanorod. (d) TEM image of the silica-coated gold nanorod. (e) Electron tomography of silica coated gold nanorods. (f) shows absorption spectra of lipoic acid-capped Ag_{29} NCs, silica-coated AuNR, and AuNR-Silica-NC composite. (g) Photographs of composite AuNR-Ag_{29} structures (i) without silica coating and (ii) with silica coating under ambient and UV light. (h) Schematic representation of AgNC-coated composite structure. (i) TEM image of AuNR-SiO_2-Ag_{29}. (j) Electron tomogram showing the 3D structure of the composite. Reproduced with permission from ref. 140 Copyright © 2022 American Chemical Society.

prevents photoluminescence quenching.[139] By controlling the thickness of silica layers, the interaction between plasmonic nanoparticles and NCs can be tuned.

Chakraborty *et al.* developed AuNR-luminescent NC multimodal imaging probes (Fig. 8c–j).[140] To fabricate the multimodal probe, a mesoporous silica shell was grown over AuNRs. The silica shell was functionalized using (3-aminopropyl) triethoxysilane (APTES). The lipoic acid (LA)-coated AgNCs ($Ag_{29}LA_{12}$) were mixed with functionalized silica-coated AuNRs to obtain composite structures (Fig. 8c and h). The resulting composite displayed a nearly two-fold increase in photoluminescence compared to that of NC alone. The approach was not limited to $Ag_{29}LA_{12}$ NCs, and similar observations were made when bovine serum albumin (BSA)-stabilized AuNCs, Au_{30}BSA was used. In both cases, the PL intensity of the NC was enhanced due to plasmonic coupling, demonstrating the generic nature of the strategy.

4.4 Dynamic covalent chemistry: toroids and supertoroidal frameworks

Most of the reports on nanoparticle-based self-assemblies offer static and equilibrium structures. Importantly, for plasmonic nanoparticles, stimuli-responsive reversible assemblies and dynamic self-assemblies have been studied. However, examples of reversible NC-based assemblies are rare in the literature. Rival *et al.* developed thiolated azobenzene-capped gold NCs showing light-triggered reversible assemblies.[141] In this approach, facile *cis–trans* isomerization and attractive dipole–dipole interactions between azobenzene molecules in the *cis* form were exploited to achieve inter-NC interaction. The thiolated azobenzene-functionalized Au_{25}NCs self-assembled into disc-like superstructures ($d \sim$ 100–1000 nm) when irradiated with UV light at 345 nm. The superstructures disassembled into individual NCs upon irradiation with 435 nm wavelength.

In biological systems, amphiphilic water-soluble cytoplasmic β-barrel proteins and transmembrane pore-forming proteins have important functions.[142a] Their amphiphilic properties have been mimicked using peptide amphiphiles to construct nanorings and microtoroidal structures.[142b–d] However, toroidal assemblies using metal nanoparticle self-assemblies have not been reported in the literature. Lakshmi *et al.* reported the dynamic covalent chemistry-driven reversible self-assembly of Au_{25} NCs into toroids and supertoroidal macroscopic frameworks (Fig. 9a–g).[143] The NCs capped with thiolated umbelliferone (7-hydroxycoumarin) ligands allowed a [2+2] cycloaddition reaction when irradiated with UV light at 365 nm (Fig. 9a). This resulted in inter-NC bonding *via* covalently linked cyclobutene adducts furnishing toroids (Fig. 9b and c). Using extensive

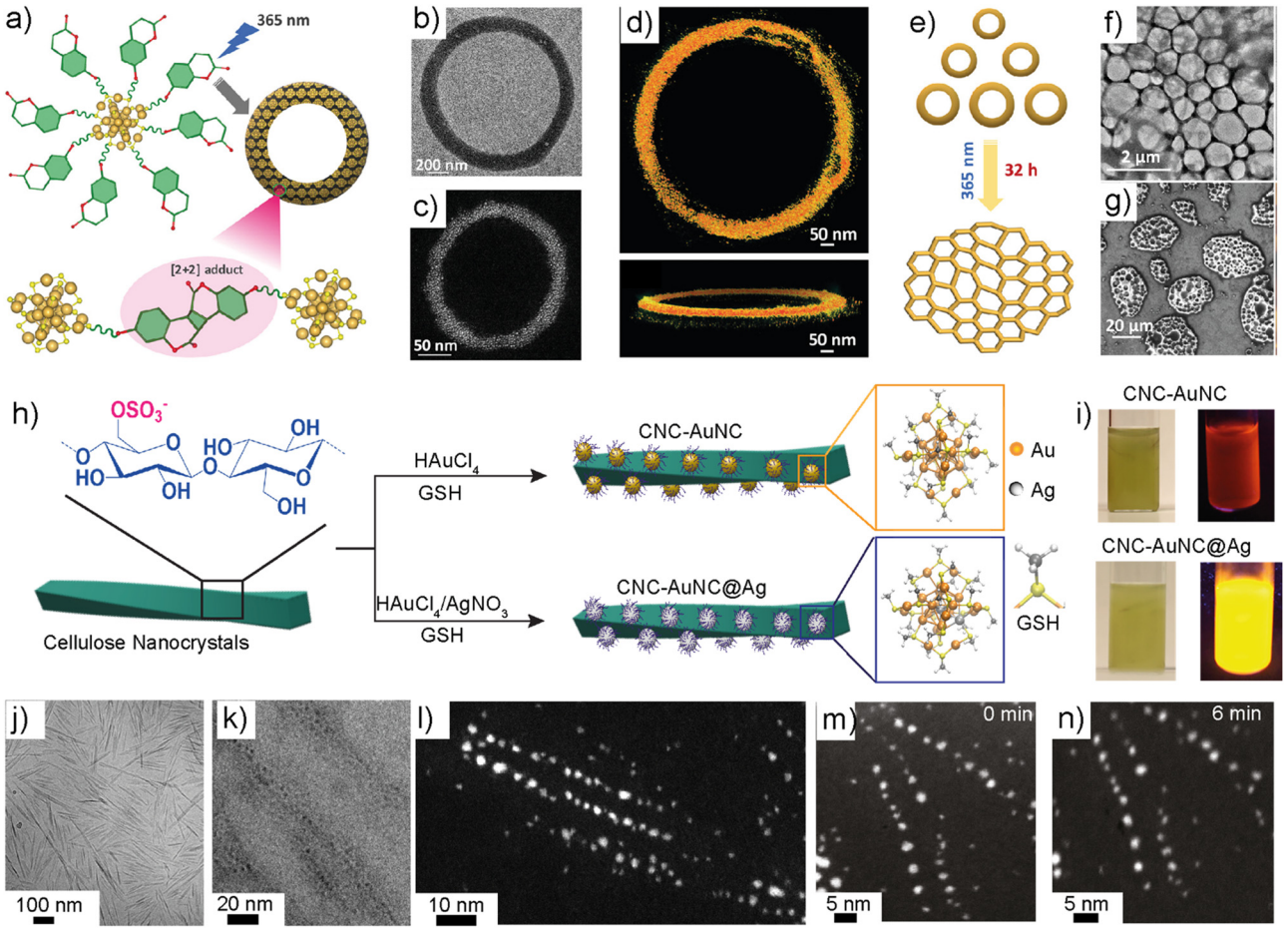

Fig. 9 Dynamic covalent chemistry, toroidal frameworks, and templated synthesis. (a) Schematic illustration of thiolated coumarin-capped Au_{25}NC. (b) and (c) TEM and DF-STEM images of a single toroid. (d) Electron tomographic reconstructed structure of a toroid. (e) Schematic illustration of light-triggered super toroidal framework formation. (f) and (g) TEM and SEM images of supertoroidal frameworks. Reproduced with permission from ref. 143 Copyright © 2023 Wiley-VCH. (h) Schematic structure of cellulose nanocrystals and the templated *in situ* synthesis of NCs. (i) Photographs showing the luminescence of *in situ*-synthesized NCs. (j) TEM image of cellulose nanocrystals. (k) The Cryo-TEM image of CNC-NC shows the NCs deposited along the CNC surface. (l) DF-STEM image of CNC-NC. (m) and (n) STEM images showing electron beam stability at 0 and 6 minutes of continuous irradiation. Reproduced with permission from ref. 148 Copyright © 2023 Wiley-VCH.

electron microscopy imaging and tomographic reconstruction, the growth mechanism of toroid formation was investigated (Fig. 9d). The photocycloaddition initially resulted in spherical aggregates that underwent further rearrangement into toroids. Continued irradiation led to the fusion of the toroids into hexagonally packed macroscopic supertoroidal frameworks (Fig. 9e–g). Due to the dynamic nature of the [2+2] cycloaddition reaction, irradiation of the toroids at 254 nm resulted in their disassembly into individual NCs. The reversible nature of the cycloaddition reaction was exploited for the conjugation of 5-fluorouracil, and controlled release. Overall, this work represents reversible covalent nanocluster-based frameworks across length scales. Furthermore, it offers routes for hierarchically porous macroscopic frameworks.

4.5 Colloidal templates and *in situ* synthesis of luminescent nanoclusters

Noble metal nanoparticles have been studied for hybrid structure formation by mixing a variety of anisotropic colloidal particles. For example, negatively charged cellulose nanocrystals (CNCs) prepared using sulfuric acid hydrolysis have been used for anchoring cationic gold nanoparticles *via* electrostatic assembly for chiral plasmonics.[144,145] CNCs also provide mechanical reinforcement for optomechanically tunable functional gels.[146] The rod-like structures with negatively charged sulfate half-ester groups offer a route for the *in situ* synthesis of NCs. Hynninen *et al.* demonstrated that glutathione-capped gold NCs can be prepared by interacting the metal precursor ($HAuCl_4{\cdot}3H_2O$) with CNCs.[147] The addition of glutathione ligands to the metal ion-deposited templates resulted in highly luminescent NCs. TEM and STEM imaging showed that the NCs were placed along the CNC surface with an inter-NC distance of ~5 nm. The inter-NC distance corresponds to the relative distance between sulfate groups. The templated NCs were used for mechanically strong luminescent bio-based optical fibers.

Selectively replacing the Au atoms with Ag atoms offers a facile route for amplified luminescence in NCs. For example, in

Au_{25}NC, the possible doping sites are the central core, outer core and staple motifs. The doping of Ni, Pd and Pt takes place at the central core of AuNC, whereas doping of Ag, Cd, Hg and Mn results in the replacement of Au atoms from the outer core. Wang *et al.* demonstrated that replacing up to 12 Au atoms in Au_{25} NCs with Ag atoms resulted in identical optical properties to that of the undoped Au_{25}NC.[79a] This is due to the exclusive doping of Ag at the outer core. However, when the 13th atom was replaced with Ag, a 200-fold increase in PL was observed due to the replacement of the core including the central Au atom. Substitution at the central core is energetically unfavourable as compared to the outer core. More importantly, NCs with excessive Ag atoms may be cytotoxic due to the leaching of Ag^+ ions when used for biological applications. Therefore, there is a need to identify new routes for the selective incorporation of a minimum number of Ag atoms to amplify optical properties.

Chandra *et al.* reported a CNC-templated approach for the core-selective doping of Au_{25}NCs (Fig. 9h and i).[148] This work demonstrated the selective replacement of the central Au atom with a Ag atom without affecting the outer core of Au_{25}NC for the first time. This was achieved by adding Ag and Au precursors to an aqueous solution containing CNCs. The $-OSO_3-$ groups on the CNC surface allowed the preferential complexation of Ag(I) ions before accumulating Au(III) complexes, furnishing NCs with the central atom doped with Ag. The resulting core-selective doped NCs displayed an absolute quantum yield of $\approx$23%. The absolute quantum yield of the templated doped NCs was 6.5 times higher than that of the undoped NCs. The TEM images revealed that the NCs were aligned along the template with an average inter-NC distance of 5.0 nm. Apart from selective doping and amplified optical properties, the NCs displayed resistance from beam damage upon continuous irradiation under STEM imaging conditions (Fig. 9l–n) The MTT assay suggested that the resulting core-doped NCs are non-toxic and non-reactive when studied against Human Dermal Fibroblasts. The role of the $-OSO_3^-$ group was further studied using DFT calculations. The generic nature of the approach was supported by a similar doping experiment using polystyrene particles. Overall, this study demonstrates, the role of colloidal templates, and the $-OSO_3$ group in selective doping to achieve optically and biologically important NCs.

5. Conclusions

Atomically precise nanoclusters are unique nanoscale building blocks due to their precise structure, composition, optical properties, and stability. Their physical properties can be tuned by adding or removing a single metal atom. While extensive studies on their structure, properties, and characterization are documented in the literature, utilizing them for self-assembled structures with long-range order is still emergent. In this feature article, the author's early attempts to exploit patchy ligand distribution, anisotropic interacting sites, and their potential use for a range of self-assembly are presented along with several examples.

It is important to note that plasmonic nanoparticle self-assembly is well established. However, they do not allow the modularity achieved using NCs. Furthermore, large nanoparticles are limited to one assembly type under narrow experimental conditions. However, using one kind of NC, multiple morphologies offering routes for diverse functional structures can be achieved. It is evident that the examples discussed in this manuscript show some of the important properties. For example, understanding the structure and chemical properties of NCs and ligands allows the design of experimental conditions to achieve desired end products. The experimental conditions can be tuned to attain discrete colloidal superstructures with a high degree of control over their size, shape, and optical properties. Since the inter-NC interactions are predominantly guided using the supramolecular interactions through ligands, the intrinsic properties of individual NCs are retained across length scales. At the same time, emergent properties were observed, such as increased quantum yield, improved biological activity, reduced toxicity, and enhanced catalytic properties.

New approaches to utilizing colloidal templates allow the synthesis of NCs that are not possible using conventional methods, paving the way for multifunctional colloidal hybrids. Overall, the self-assembly of NCs is yet to fulfil its potential for further applications such as device fabrication. With the wealth of structural data and increasing self-assembled structures, further efforts are needed to meet the goal of precision nanoengineering. For example, various computational simulation studies have been used to understand nanoclusters' structure and optical properties. However, more effort must be made to use computational simulations to understand or predict the self-assembly of NCs. Computational simulations will play a significant role in predictive structure formation together with rapidly evolving machine learning algorithms and artificial intelligence tools. Combining experimental data and simulations will lead to a breakthrough in precision nanoengineering and provide new avenues for atomically precise manufacturing of macroscopic materials.

Conflicts of interest

There are no conflicts to declare.

Acknowledgements

Academy of Finland for project funding (No. 352900) and Flagship program on Photonics Research and Innovation (PREIN) are acknowledged. The author thanks all collaborators and co-authors (whose names appear in the cited references) involved in exploring nanocluster self-assembly. Their contributions were crucial in advancing the topics discussed in this feature article.

Notes and references

1 (*a*) L. Pokrajac, A. Abbas, W. Chrzanowski, G. M. Dias, B. J. Eggleton, S. Maguire, E. Maine, T. Malloy, J. Nathwani, L. Nazar, A. Sips, J. Sone, A. van den Berg, P. S. Weiss and S. Mitra, *ACS Nano*,

2021, **15**, 18608–18623; (*b*) D. J. McClements, *ACS Omega*, 2020, **5**, 29623–29630; (*c*) J. Yan, B. K. Teo and N. Zheng, *Acc. Chem. Res.*, 2018, **51**(12), 3084–3093; (*d*) K. W. Guo, *Int. J. Energy Res.*, 2012, **36**, 1–17.
2 M. J. Mitchell, M. M. Billingsley, R. M. Haley, M. E. Wechsler, N. A. Peppas and R. Langer, *Nat. Rev. Drug Discovery*, 2021, **20**, 101–124.
3 W. S. Zhi, J. Kibsgaard, F. D. Colin, I. Chorkendorff, K. N. Jens and F. J. Thomas, *Science*, 2017, **355**, eaad4998.
4 (*a*) R. Jin, Y. Pei and T. Tsukuda, *Acc. Chem. Res.*, 2019, **52**, 1; (*b*) Q. Yao, Q. Zhang and J. Xie, *Ind. Eng. Chem. Res.*, 2022, **61**, 7594–7612.
5 D. R. Danielsen, A. Lyksborg-Andersen, K. E. S. Nielsen, B. S. Jessen, T. J. Booth, M.-H. Doan, Y. Zhou, P. Bøggild and L. Gammelgaard, *ACS Appl. Mater. Interfaces*, 2021, **13**, 41886–41894.
6 D. Guo, G. Xie and J. Luo, *J. Phy. D: Appl. Phys.*, 2014, **47**, 013001.
7 (*a*) C. M. Aikens, *Acc. Chem. Res.*, 2018, **51**, 3065–3073; (*b*) M. R. Friedfeld, J. L. Stein, A. Ritchhart and B. M. Cossairt, *Acc. Chem. Res.*, 2018, **51**, 2803–2810; (*c*) C. Lionello, C. Perego, A. Gardin, R. Klajn and G. M. Pavan, *ACS Nano*, 2023, **17**, 275–287.
8 P. Chakraborty, A. Nag, A. Chakraborty and T. Pradeep, *Acc. Chem. Res.*, 2019, **52**, 2–11.
9 (*a*) Y. Suzuki, G. Cardone, D. Restrepo, P. D. Zavattieri, T. S. Baker and F. A. Tezcan, *Nature*, 2016, **533**, 369–373; (*b*) H. Liu, Z. Lu, B. Tang, C. Qu, Z. Zhang and H. Zhang, *Angew. Chem., Int. Ed.*, 2020, **59**, 12944–12950; (*c*) B. Bhattacharya, D. Roy, S. Dey, A. Puthuvakkal, S. Bhunia, S. Mondal, R. Chowdhury, M. Bhattacharya, M. Mandal, K. Manoj, P. K. Mandal and C. M. Reddy, *Angew. Chem., Int. Ed.*, 2020, **59**, 19878–19883.
10 (*a*) P. Kissel, D. J. Murray, W. J. Wulftange, V. J. Catalano and B. T. King, *Nat. Chem.*, 2014, **6**, 774–778; (*b*) M. J. Kory, M. Wörle, T. Weber, P. Payamyar, S. W. van de Poll, J. Dshemuchadse, N. Trapp and A. D. Schlüter, *Nat. Chem.*, 2014, **6**, 779–784.
11 A. von Hippel, *Science*, 1956, **123**, 315–317.
12 (*a*) K. E. Drexler, *Proc. Natl. Acad. Sci. U. S. A.*, 1981, **78**, 5275–5278; (*b*) G. Zaldivar, Y. A. P. Sirkin, G. Debais, M. Fiora, L. L. Missoni, E. G. Solveyra and M. Tagliazucchi, *ACS Omega*, 2022, **7**(43), 38109–38121.
13 (*a*) X. Xing, Z. Man, J. Bian, Y. Yin, W. Zhang and Z. Lu, *Nat. Commun.*, 2020, **11**, 6002; (*b*) S. Jesse, A. Y. Borisevich, J. D. Fowlkes, A. R. Lupini, P. D. Rack, R. R. Unocic, B. G. Sumpter, S. V. Kalinin, A. Belianinov and O. S. Ovchinnikova, *ACS Nano*, 2016, **10**, 5600–5618.
14 G. M. Whitesides and M. Boncheva, *Proc. Natl. Acad. Sci. U. S. A.*, 2002, **99**, 4769–4774.
15 (*a*) K. E. B. Doncom, L. D. Blackman, D. B. Wright, M. I. Gibson and R. K. O'Reilly, *Chem. Soc. Rev.*, 2017, **46**, 4119–4134; (*b*) V. N. Manoharan, *Science*, 2015, **349**, e1253751.
16 S. Hiraoka, *Bull. Chem. Soc. Jpn.*, 2018, **91**, 957–978.
17 D. Moatsu and R. K. O'Reilly, *Chem*, 2019, **5**, 487–490.
18 (*a*) O. Ikkala and G. ten Brinke, *Chem. Commun.*, 2004, 2131–2137; (*b*) L. Li, K. Raghupathi, C. Song, P. Prasad and S. Thayumanavan, *Chem. Commun.*, 2014, **50**, 13417–13432.
19 (*a*) T. Pelras, C. S. Mahon, Nonappa, O. Ikkala, A. H. Gröschel and M. Müllner, *J. Am. Chem. Soc.*, 2018, **140**, 12736–12740; (*b*) T. Pelras, Nonappa, C. S. Mahon and M. Müllner, *Macromol. Rapid Commun.*, 2021, **42**, 2000401.
20 (*a*) Y. Xia, T. D. Nguyen, M. Yang, B. Lee, A. Santos, P. Podsiadlo, Z. Tang, S. C. Glotzer and N. A. Kotov, *Nat. Nanotechnol.*, 2011, **6**, 580–587; (*b*) N. A. Kotov, *Europhys. Lett.*, 2017, **119**, 6(c).
21 A. Rao, S. Roy, V. Jain and P. Pillai, *ACS Appl. Mater. Interfaces*, 2022, **15**, 25248–25274.
22 (*a*) M. M. Nigra, J.-M. Ha and A. Katz, *Catal. Sci. Technol.*, 2013, **3**, 2976–2983; (*b*) Y. Zhao, Y. Huang, H. Zhu, Q. Zhu and Y. Xia, *J. Am. Chem. Soc.*, 2016, **138**, 16645–16654; (*c*) N. Sarfraz and I. Khan, *Chem. – Asian J.*, 2021, **16**, 720–742; (*d*) Z. Xu, Y. Li, G. Gao, F. Xie, R. Ju, S. Yu, K. Liu, J. Li, W. Wang, W. Li, T. Li and C.-W. Qiu, *APL Photonics*, 2023, **8**, 020801; (*e*) K. Bian, H. Schunk, D. Ye, A. Hwang, T. S. Luk, R. Li, Z. Wang and H. Fan, *Nat. Commun.*, 2018, **9**, 2365; (*f*) T. D. Tran, A. M. T. T. Nguyen, H. V. Le, D. N. Nguyen, Q. D. Truong and P. D. Tran, *Chem. Commun.*, 2018, **54**, 3363–3366; (*g*) N. S. Thakur, G. Patel, V. Kushwah, S. Jain and U. C. Banerjee, *ACS Appl. Bio Mater.*, 2019, **2**, 349–361; (*h*) S. Park, W. J. Lee, S. Park, D. Choi, S. Kim and N. Park, *Sci. Rep.*, 2019, **9**, 20180; (*i*) S. Yang, D. Yao, Y. Wang, W. Yang, B. Zhang and D. Wang, *Chem. Commun.*, 2018, **54**, 9841–9844.
23 (*a*) Y. Wang, O. Zeiri, M. Raula, B. Le Ouay, F. Stellacci and I. A. Weinstock, *Nat. Nanotechnol.*, 2016, **12**, 170–176; (*b*) H. Zhao, S. Sen, T. Udayabhaskararao, M. Sawczyk, K. Kučanda, D. Manna, P. K. Kundu, J.-W. Lee, P. Král and R. Klajn, *Nat. Nanotechnol.*, 2016, **11**, 82–88; (*c*) C. Pigliacelli, D. Maiolo, Nonappa, J. S. Haataja, H. Amenitsch, C. Michelet, P. S. Moreno, I. Tirotta, P. Metrangolo and F. B. Bombelli, *Angew. Chem., Int. Ed.*, 2017, **56**, 16186–16190.
24 M. S. Lee, D. W. Yee, M. Ye and R. J. Macfarlane, *J. Am. Chem. Soc.*, 2022, **144**, 3330–3346.
25 W. Zhang, Nanoparticle Aggregation: Principles and Modeling, in *Nanomaterial. Advances in Experimental Medicine and Biology*, ed. D. Capco and Y. Chen, Springer, Dordrecht, 2014, 811, pp. 19–43.
26 D. Luo, C. Yan and T. Wang, *Small*, 2015, **11**, 5984–6008.
27 S. Shrestha, B. Wang and P. Dutta, *Adv. Colloid Interface Sci.*, 2020, **279**, 102162.
28 X. Zhang, L. Lv, L. Ji, G. Guo, L. Liu, D. Han, B. Wang, Y. Tu, J. Hu, D. Yang and A. Dong, *J. Am. Chem. Soc.*, 2016, **138**, 3290–3293.
29 Z. Tang and N. A. Kotov, *Adv. Mater.*, 2005, **17**, 951–962.
30 L. Chen, B. Su and L. Jang, *Chem. Soc. Rev.*, 2019, **48**, 8–21.
31 X. Xue, K. Liu and E. P. Furlani, *J. Phys. Chem. C*, 2017, **121**, 9489–9496.
32 S. Cheng and G. S. Grest, *ACS Macro Lett.*, 2016, **5**, 694–698.
33 (*a*) P. Katiyar and J. K. Singh, *J. Chem. Phys.*, 2019, **150**, 044708; (*b*) S. Cheng and G. S. Grest, *J. Chem. Phys.*, 2013, **138**, 064701; (*c*) J. Ku, D. M. Aruguete, A. P. Alivisatos and P. L. Geissler, *J. Am. Chem. Soc.*, 2011, **133**, 838–848; (*d*) E. Rabani, D. R. Reichman, P. L. Geissler and L. E. Brus, *Nature*, 2003, **426**, 271–274; (*e*) P. Guo and Y. Gao, *Phys. Rev. Lett.*, 2020, **124**, 066101; (*f*) Y. Zhou, T.-Y. Tang, B. H.-J. Lee and G. Arya, *ACS Nano*, 2022, **16**, 7457–7470.
34 H. Jia, Y.-F. Zhang, C. Zhang, M. Ouyang and S. Du, *J. Phys. Chem. B*, 2023, **127**, 2258–2266.
35 (*a*) Y. Sun and Y. Xia, *Science*, 2002, **298**, 2176–2179; (*b*) K. An and G. A. Somorjai, *ChemCatChem*, 2012, **4**, 1512–1524; (*c*) M. L. Personick and C. A. Mirkin, *J. Am. Chem. Soc.*, 2013, **135**, 18238–18247; (*d*) J. Piella, N. G. Bastús and V. Puntes, *Chem. Mater.*, 2016, **28**, 1066–1075.
36 (*a*) A. M. Kalsin, M. Fialkowski, M. Paszewski, S. K. Smoukov, K. J. M. Bishop and B. A. Grzybowski, *Science*, 2006, **312**, 420–424; (*b*) R. Klajn, K. J. M. Bishop and B. A. Grzybowski, *Proc. Natl. Acad. Sci. U. S. A.*, 2007, **104**, 10305–10309; (*c*) D. Nykypanchuk, M. M. Maye, D. van der Lelie and O. Gang, *Nature*, 2008, **451**, 549–552; (*d*) S. Y. Park, A. K. R. Lytton-Jean, B. Lee, S. Weigand, G. C. Schatz and C. A. Mirkin, *Nature*, 2008, **451**, 553–556.
37 (*a*) R. A. Alvarez-Puebla, A. Agarwal, P. Manna, B. P. Khanal, P. Aldeanueva-Potel, E. Carbó-Argibay, N. Pazos-Pérez, L. Vigderman, E. R. Zubarev, N. A. Kotov and L. M. Liz-Marzán, *Proc. Natl. Acad. Sci. U. S. A.*, 2011, **108**, 8157–8161; (*b*) P. P. Pillai, B. Kowalczyk and B. A. Grzybowski, *Nanoscale*, 2016, **8**, 157–161; (*c*) P. J. Santos, P. A. Gabrys, L. Z. Zornberg, M. S. Lee and R. J. Macfarlane, *Nature*, 2021, **591**, 586–591; (*d*) J. Wang, T. S. Peled and R. Klajn, *J. Am. Chem. Soc.*, 2023, **145**(7), 4098–4108.
38 (*a*) T. P. Bigioni, X.-M. Lin, T. T. Nguyen, E. I. Corwin, T. A. Witten and H. M. Jaeger, *Nat. Mater.*, 2006, **5**, 265–270; (*b*) K. E. Mueggenburg, X.-M. Lin, R. H. Goldsmith and H. M. Jaeger, *Nat. Mater.*, 2007, **6**, 656–660; (*c*) W. Cheng, M. J. Campolongo, J. J. Cha, S. J. Tan, C. C. Umbach, D. A. Muller and D. Luo, *Nat. Mater.*, 2009, **8**, 519–525; (*d*) A. Dong, J. Chen, P. M. Vora, J. M. Kikkawa and C. B. Murray, *Nature*, 2010, **466**, 474–477; (*e*) A. Desireddy, C. P. Joshi, M. Sestak, S. Little, S. Kumar, N. J. Podraza, S. Masillac, R. W. Collins and T. P. Bigioni, *Thin Solid Films*, 2011, **519**, 6077–6084; (*f*) W. Cheng, M. J. Campolongo, J. J. Cha, S. J. Tan, C. C. Umbach, D. A. Muller and D. Luo, *Nat. Mater.*, 2009, **8**, 519.
39 N. A. Kotov, *Science*, 2010, **330**, 188–189.
40 J.-Y. Kim and N. A. Kotov, *Science*, 2019, **365**, 1378–1379.
41 N. A. Kotov, L. M. Liz-Marzán and Q. Wang, *Mater. Adv.*, 2022, **3**, 3677–3679.
42 A. Nag, P. Chakraborty, G. Paramasivam, M. Bodiuzzaman, G. Natarajan and T. Pradeep, *J. Am. Chem. Soc.*, 2018, **140**, 13590–13593.
43 (*a*) F. Alibart, S. Pleutin, D. Guérin, C. Novembre, S. Lenfant, K. Lmimouni, C. Gamrat and D. Vuillaume, *Adv. Funct. Mater.*,

2010, **22**, 330; (*b*) F. Alibert, S. Pleutin, O. Bichler, C. Gamrat, T. Serrano-Gotarrendona, B. Linares-Barranco and D. Vuillaume, *Adv. Funct. Mater*, 2012, **8**, 609.
44 W. J. Cho, Y. Kim and J. K. Kim, *ACS Nano*, 2012, **6**, 249.
45 (*a*) J. N. Randall, J. R. Von Ehr, J. Ballard, J. Owen, R. Saini, E. Fuchs, H. Xu and S. Chen, Atomically Precise Manufacturing: The Opportunity, Challenges, and Impact, in *Atomic Scale Interconnection Machines. Advances in Atom and Single Molecule Machines*, ed. C. Joachim, Springer, Berlin, Heidelberg, 2012, pp. 89–106; (*b*) J. N. Randall, J. H. G. Owen, E. Fuchs, J. Lake, J. R. Von Her, J. Ballard and E. Henriksen, *Micro Nano Eng.*, 2018, **1**, 1–14; (*c*) F. Fang, N. Zhang, D. Guo, K. Ehmann, B. Cheung, K. Liu and K. Yamamura, *Int. J. Extrem. Manuf.*, 2019, **1**, 012001.
46 (*a*) S. Umbrello and S. D. Baum, *Futures*, 2018, **100**, 63–73; (*b*) S. Knappe, V. Shah, P. Schwindt, L. Hollberg, J. Kitching, L.-A. Liew and J. Moreland, *Appl. Phys. Lett.*, 2004, **85**, 1460–1462.
47 D. M. Eigler and E. K. Schweizer, *Nature*, 1990, **344**, 524–526.
48 (*a*) X. Xing, Z. Man, J. Bian, Y. Yin, W. Zhang and Z. Lu, *Nat. Commun.*, 2020, **11**, 6002; (*b*) S. Jesse, A. Y. Borisevich, J. D. Fowlkes, A. R. Lupini, P. D. Rack, R. R. Unocic, B. G. Sumpter, S. V. Kalinin, A. Belianinov and O. S. Ovchinnikova, *ACS Nano*, 2016, **10**, 5600–5618.
49 (*a*) K. P. Velikov, C. G. Christova, R. P. A. Dullens and A. van Blaaderen, *Science*, 2002, **296**, 106–109; (*b*) W. Poon, *Science*, 2004, **304**, 830–831.
50 (*a*) V. N. Manoharan, M. T. Elsesser and D. J. Pine, *Science*, 2003, **301**, 483–487; (*b*) Y. Wang, Y. Wang, D. R. Breed, V. N. Manoharan, L. Feng, A. D. Hollingsworth, M. Weck and D. J. Pine, *Nature*, 2012, **491**, 51–55; (*c*) A. van Blaaderen, *Science*, 2003, **301**, 470–471.
51 D. Morphew and D. Chakrabarti, *Curr. Opin. Colloid Interface Sci.*, 2017, **30**, 70–80.
52 (*a*) P. L. Biancaniello, A. J. Kim and J. C. Crocker, *Phys. Rev. Lett.*, 2005, **94**, 058302; (*b*) D. J. Kraft, J. Groenewold and W. K. Kegel, *Soft Matter*, 2009, **5**, 3823–3826.
53 D. Morphew, J. Shaw, C. Avins and D. Chakrabarti, *ACS Nano*, 2018, **12**, 2355–2364.
54 (*a*) J. Opdam, R. Tuinier, T. Hueckel, T. J. Snoeren and S. Sacanna, *Soft Matter*, 2020, **16**, 7438–7446; (*b*) X. Zhou, D. Yao, W. Hua, N. Huang, X. Chen, L. Li, M. He, Y. Zhang, Y. Guo, S. Xiao, F. Bian and H. Liang, *Proc. Natl. Acad. Sci. U. S. A.*, 2020, **117**, 5617–5623; (*c*) B. Luo, A. Kim, J. W. Smith, Z. Ou, Z. Wu, J. Kim and Q. Chen, *Nat. Commun.*, 2019, **10**, 1815.
55 (*a*) A. B. Rao, J. Shaw, A. S. Neophytou, D. Morphew, F. Sciortino, R. L. Johnston and D. Chakrabarti, *ACS Nano*, 2020, **14**, 5348–5359; (*b*) A. Neophytou, V. N. Manoharan and D. Chakrabarti, *ACS Nano*, 2021, **15**, 2668–2678.
56 (*a*) in *Protected Metal Clusters from Fundamentals to Applications in Frontiers of Nanoscience* ed. T. Tsukuda and H. Häkkinen, Elsevier Inc., 2015, **9**, pp. 1–358; (*b*) in *Atomically Precise Metal Nanoclusters*, ed. T. Pradeep, Elsvier Inc., 2022, pp. 1–643; (*c*) R. Jin and D. Jiang, *Atomically Precise Nanochemistry*, Wiley-VCH, 2023, pp. 1–528.
57 (*a*) R. Jin, C. Zeng, M. Zhou and Y. Chen, *Chem. Rev.*, 2016, **116**, 10346–10413; (*b*) Y. Du, H. Sheng, D. Astruc and M. Zhu, *Chem. Rev.*, 2020, **120**, 526–622; (*c*) X. Kang, Y. Li, M. Zhu and R. Jin, *Chem. Soc. Rev.*, 2020, **49**, 6443–6514; (*d*) J. Yang and R. Jin, *ACS Mater. Lett.*, 2019, **1**, 482–489; (*e*) I. Chakraborty and T. Pradeep, *Chem. Rev.*, 2017, **117**, 8208–8271.
58 H. Häkkinen, *Nat. Chem.*, 2012, **4**, 443–455.
59 (*a*) L. Malatesta, L. Naldini, G. Simonetta and F. Cariati, *Chem. Commun.*, 1965, 212–213; (*b*) L. Naldini, F. Cariati, G. Simonetta and L. Malatesta, *Chem. Commun.*, 1966, 647–648; (*c*) M. McPartlin and R. Mason, *Chem. Commun.*, 1969, 334; (*d*) P. A. Bartlett and B. B. S. J. Sanger, *J. Am. Chem. Soc.*, 1978, 5085.
60 D. Safer, L. Bolinger and J. S. Leigh Jr., *J. Inorg. Biochem.*, 1986, **26**, 77–91.
61 (*a*) G. Schmid, R. Pfeil, R. Boese, F. Bandermann, S. Meyer, G. H. M. Calis and J. W. A. van der Velden, *Chem. Ber.*, 1981, **114**, 3634–3642; (*b*) D. M. P. Mingos, *Struct. Bond*, 2014, **161**, 117–154.
62 M. Brust, M. Walker, D. Bethell, D. J. Schiffrin and R. Whyman, *J. Chem. Soc., Chem. Commun.*, 1994, 801–802.
63 Y. Negishi, K. Nobusada and T. Tsukuda, *J. Am. Chem. Soc.*, 2005, **127**, 5261–5270.
64 Z. Wu and R. Jin, *Atomically Precise Metal Nanoclusters*, Springer International Publishing, Cham, 2021, pp. 31–78.
65 P. D. Jadzinsky, G. Calero, C. J. Ackerson, D. A. Bushnell and R. D. Kornberg, *Science*, 2007, **318**, 430–433.
66 M. Zhu, C. M. Aikens, F. J. Hollander, G. C. Schatz and R. Jin, *J. Am. Chem. Soc.*, 2008, **130**, 5883–5885.
67 C. Pigliacelli, A. Acocella, I. Díez, L. Moretti, V. Dichiarante, N. Demitri, H. Jiang, M. Maiuri, R. H. A. Ras, F. B. Bombelli, G. Cerullo, F. Zerbetto, P. Metrangolo and G. Terraneo, *Nat. Commun.*, 2022, **13**, 2607.
68 (*a*) M. Azubel, J. Koivisto, S. Malola, D. Bushnell, G. L. Hura, A. L. Koh, H. Tsunoyama, T. Tsukuda, M. Pettersson, H. Häkkinen and R. D. Kornberg, *Science*, 2014, **345**, 909–911; (*b*) M. Azubel, A. L. Koh, K. Koyasu, T. Tsukuda and R. D. Kornberg, *ACS Nano*, 2017, **11**, 11866–11871.
69 S. Vergara, D. A. Lukes, M. W. Martynowycz, U. Santiago, G. Plascencia-Villa, S. C. Weiss, M. J. de la Cruz, D. M. Black, M. M. Alvarez, X. López-Lozano, C. O. Barnes, G. Lin, H.-C. Weissker, R. L. Whetten, T. Gonen, M. J. Yacaman and G. Calero, *J. Phys. Chem. Lett.*, 2017, **8**, 5523–5530.
70 P. Chakraborthy and T. Pradeep, *NPG Asia Mater.*, 2019, **11**, 48.
71 K. Salorinne, S. Malola, O. A. Wong, C. D. Rithner, X. Chen, C. J. Ackersonand and H. Häkkinen, *Nat. Commun.*, 2016, **7**, 10401.
72 (*a*) D. M. Chevrier, R. Yang, A. Chatt and P. Zhang, *Nanotechnol. Rev.*, 2015, **4**, 193–206; (*b*) E. Bolli, A. Mezzi, L. Burratti, P. Prosposito, S. Casciardi and S. Kaciulis, *Surf. Interface Anal.*, 2020, **52**, 1017–1022.
73 (*a*) H. Kang and M. Zhu, *Chem. Soc. Rev.*, 2019, **48**, 2422–2457; (*b*) H. Qian, M. Y. Sfeir and R. Jin, *J. Phys. Chem. C*, 2010, **114**, 19935–19940; (*c*) S. H. Yau, O. Varnavski and T. G. Ill, *Acc. Chem. Res*, 2013, **46**, 1506–1516.
74 C. Zeng, Y. Chen, K. Kirschbaun, K. J. Lambright and R. Jin, *Science*, 2016, **354**, 1580–1584.
75 (*a*) K. S. Sugi, P. Bandyopadhyay, M. Bodiuzzaman, A. Nag, M. Hridya, W. A. Dar, P. Ghosh and T. Pradeep, *Chem. Mater.*, 2020, **32**, 7973–7984; (*b*) K. S. Sugi, A. Maier and M. Scheele, *Chem. Commun.*, 2022, **58**, 6998–7107.
76 X. Du and R. Jin, *ACS Nano*, 2019, **13**, 7383–7738.
77 S. Zhao, R. Jin, Y. Song, H. Zhang, S. D. House, J. C. Yang and R. Jin, *Small*, 2017, **13**, 1701519.
78 (*a*) S. Li, A. V. Nagarajan, D. R. Alfonso, M. Sun, D. R. Kauffman, G. Mpourmpakis and R. Jin, *Angew. Chem., Int. Ed.*, 2021, **60**, 6351–6356; (*b*) X. Cai, G. Li, W. Hu and Y. Zhu, *ACS Catal*, 2022, **12**, 10638–10653.
79 (*a*) S. Wang, X. Meng, A. Das, T. Li, Y. Song, T. Cao, X. Zhu, M. Zhu and R. Jin, *Angew. Chem., Int. Ed.*, 2014, **53**, 2376; (*b*) L. Chen, A. Black, W. J. Parak, C. Klinke and I. Chakraborty, *Aggregate*, 2022, **3**, e132; (*c*) S. Chandra, A. Sciortino, S. Das, F. L. Ahmed, A. Jana, J. Roy, D. Li, V. Liljeström, H. Jiang, L.-S. Johansson, X. Chen, Nonappa, M. Cannas, T. Pradeep, B. Peng, R. H. A. Ras, Z. Sun, O. Ikkala and F. Messina, *Adv. Opt. Mater.*, 2023, **11**, 2202649.
80 (*a*) V. Jeseentharani, N. Pugazhenthiran, A. Mathew, I. Chakraborty, A. Baksi, J. Ghosh, M. Jash, G. S. Anjusree, T. G. Deepak, A. S. Nair and T. Pradeep, *ChemistrySelect*, 2017, **2**, 1454–1463; (*b*) K. G. Stamplecoskie and A. Swint, *J. Mater. Chem. A*, 2016, **4**, 2075–2081.
81 (*a*) M. McPartlin and R. Mason, *Chem. Commun.*, 1969, 334; (*b*) P. A. Bartlett, B. Bauer and S. J. Singer, *J. Am. Chem. Soc.*, 1978, **100**, 5085–5089.
82 (*a*) D. Safer, J. Hainfeld, J. Wall and J. Reardon, *Science*, 1982, **218**, 290; (*b*) J. E. Reardon and P. A. Frey, *Biochem.*, 1984, **23**, 3849–3856; (*c*) D. Safer, L. Bolinger and J. S. Leigh Jr., *J. Inorg. Biochem.*, 1986, **26**, 77–91.
83 (*a*) J. F. Hainfeld, *Nature*, 1988, **333**, 281–282; (*b*) T. Takizawa and J. M. Robinson, *J. Histochem. Cytochem.*, 1994, **42**, 1615–1623.
84 G. Zuber, E. Weiss and M. Chiper, *Nanotechnol.*, 2019, **30**, 352001.
85 J. V. Rival, P. Mymoona, K. M. Lakshmi, Nonappa, T. Pradeep and E. S. Shibu, *Small*, 2021, **17**, 2005718.
86 Nonappa and O. Ikkala, *Adv. Funct. Mater.*, 2018, **28**, 1704328.
87 (*a*) G. Schmid, R. Pugin, T. Sawitowski, U. Simon and B. Marler, *Chem. Commun.*, 1999, 1303–1304; (*b*) G. Schmid, M. Bäumle and N. Beyer, *Angew. Chem., Int. Ed.*, 2000, **39**, 181.
88 T. Laaksonen, P. Ahonen, C. Johans and K. Kontturi, *ChemPhysChem*, 2006, **7**, 2143–2149.
89 M. J. Cowan, T. Higaki, R. Jin and G. Mpourmpakis, *J. Phys. Chem. C*, 2019, **123**, 20006–20012.

90 (*a*) J. Kao, P. Bai, J. M. Lucas, A. P. Alivisatos and T. Xu, *J. Am. Chem. Soc.*, 2013, **135**, 1680–1683; (*b*) F. Schulz, S. Tober and H. Lange, *Langmuir*, 2017, **33**, 14437–14444.
91 (*a*) B. Derjaguin, *Acta Phys. Chim. U.S.S.R.*, 1939, **10**, 333; (*b*) B. Derjaguin and L. D. Landau, *Acta Phys. Chim. U.S.S.R.*, 1941, **14**, 633; (*c*) E. J. W. Verwey and J. T. G. Overbeek, *Theory of Stability of Lyophobic Colloids*, Elsevier, Amsterdam, The Netherlands, 1948.
92 J. H. Adair, E. Suvaci and J. Sindel, Surface and Colloid Chemistry, ed. K. H. J. Buschow, R. W. Cahn, M. C. Flemings, B. Ilschner, E. J. Kramer, S. Mahajan and P. Veyssière, in *Encyclopedia of Materials: Science and Technology*, Elsevier, 2001, pp. 1–10.
93 (*a*) Y. Liang, N. Hilal, P. Langston and V. Starov, *Adv. Colloid Interface Sci.*, 2007, **134–135**, 151–166; (*b*) Y. S. Lee, *Self-Assembly and Nanotechnology: A Force Balance Approach*, John Wiley & Sons, Inc., Hoboken, USA, 2008.
94 M. Boström, V. Deniz, G. V. Franks and B. W. Ninham, *Adv. Colloid Interface Sci.*, 2006, **123–126**, 5–15.
95 T. M. Mohona, A. Gupta, A. Masud, S.-C. Chien, L.-C. Lin, P. C. Nalam and N. Aich, *Environ. Sci. Technol.*, 2019, **53**, 4161–4172.
96 M. Boström, D. R. M. Williams and B. W. Ninham, *Phys. Rev. Lett.*, 2001, **87**, 168103.
97 A. Klug and D. L. D. Caspar, *Adv. Virus Res.*, 1960, **13**, 1–63.
98 M. G. Rossmann, *Quarter. Rev. Biophys.*, 2013, **46**, 133–180.
99 H. R. Crane, *Sci. Monthly*, 1950, **70**, 376–389.
100 (*a*) D. L. D. Caspar, *Adv. Prot. Chem.*, 1963, **18**, 37–121; (*b*) D. L. D. Caspar and A. Klug, *Cold Spring Harb. Symp. Quant. Biol.*, 1962, **27**, 1–24.
101 F. H. C. Crick and J. D. Watson, *Nature*, 1956, **177**, 473–475.
102 D. J. Kushner, *Bacteriol. Rev.*, 1969, **33**, 302–345.
103 (*a*) D. L. D. Caspar, *Adv. Protein Chem.*, 1964, **18**, 37; (*b*) W. H. Roos, R. Bruinsma and G. J. L. Wuite, *Nat. Phys.*, 2010, **6**, 733–743.
104 J. A. Speir, S. Munshi, G. Wang, T. S. Baker and J. E. Johnson, *Structure*, 1995, **3**, 63–78.
105 (*a*) L. Travaglini, A. D'Annibale, M. C. di Gregorio, K. Schillén, U. Olsson, S. Sennato, N. V. Pavel and L. Galantini, *J. Phys. Chem. B*, 2013, **117**, 9248–9257; (*b*) Z. Özdemir, D. Šaman, K. Bertula, M. Lahtinen, L. Bednárová, M. Pazderková, L. Rárová, Nonappa and Z. Wimmer, *Langmuir*, 2021, **37**(8), 2693–2706; (*c*) Z. Özdemir, D. Saman, L. Bednarova, M. Pazderkova, L. Janovska, Nonappa and Z. Wimmer, *ACS Appl. Nano Mater.*, 2022, **5**, 3799–3810; (*d*) Z. Özdemir, Nonappa and Z. Wimmer, *ACS Appl. Nano Mater.*, 2022, **5**, 16264–16277.
106 V. Linko, H. Zhang, Nonappa, M. A. Kostiainen and O. Ikkala, *Acc. Chem. Res.*, 2022, **55**, 1785–1795.
107 Y. Levi-Kalisman, P. D. Jadzinsky, N. Kalisman, H. Tsunoyama, T. Tsukuda, D. A. Bushnell and R. D. Kornberg, *J. Am. Chem. Soc.*, 2011, **133**, 2976–2982.
108 K. Salorinne, S. Malola, O. A. Wong, C. D. Rithner, X. Chen, C. J. Ackerson and H. Häkkinen, *Nat. Commun.*, 2016, **7**, 10401.
109 J. Koivisto, X. Chen, S. Donnini, T. Lahtinen, H. Häkkinen, G. Groenhof and M. Pettersson, *J. Phys. Chem. C*, 2016, **120**, 10041–10050.
110 Nonappa, T. Lahtinen, J. S. Haataja, T.-R. Tero, H. Häkkinen and O. Ikkala, *Angew. Chem., Int. Ed.*, 2016, **55**, 16035–16038.
111 A. Desireddy, B. E. Conn, J. Guo, B. Yoon, R. N. Barnett, B. M. Monahan, K. Kirschbaum, W. P. Griffith, R. L. Whetten, U. Landman and T. P. Bigioni, *Nature*, 2013, **501**, 399–402.
112 B. Yoon, W. D. Luedtke, R. N. Barnett, J. Gao, A. Desireddy, B. E. Conn, T. Bigioni and U. Landman, *Nat. Mater.*, 2014, **13**, 807–811.
113 A. Som, I. Chakraborty, T. A. Maark, S. Bhat and T. Pradeep, *Adv. Mater.*, 2016, **28**, 2827–2833.
114 A. Som, A. Griffo, I. Chakraborty, H. Hähl, B. Mondal, A. Chakraborty, K. Jacobs, P. Laaksonen, O. Ikkala, T. Pradeep and Nonappa, *Small*, 2022, **18**, 2201707.
115 J.-M. Nam, J.-W. Oh, H. Lee and Y. D. Suh, *Acc. Chem. Res.*, 2016, **49**, 2746–2755.
116 (*a*) A. K. Boal, F. Ilhan, J. E. DeRouchey, T. Thurn-Albrecht, T. P. Russell and V. M. Rotello, *Nature*, 2000, **404**, 746–748; (*b*) D. Liu, F. Zhou, C. Li, T. Zhang, H. Zhang, W. Cai and Y. Li, *Angew. Chem., Int. Ed.*, 2015, **54**, 9596–9600; (*c*) C. Pigliacelli, K. B. Sanjeeva, Nonappa, A. Pizzi, A. Gori, F. B. Bombelli and P. Metrangolo, *ACS Nano*, 2019, **13**, 2158–2166; (*d*) V. Dichiarante, C. Pigliacelli, P. Metrangolo and F. B. Bombelli, *Chem. Sci.*, 2021, **12**, 1632–1646.
117 Nonappa, J. S. Haataja, J. V. I. Timonen, S. Malola, P. Engelhardt, N. Houbenov, M. Lahtinen, H. Häkkinen and O. Ikkala, *Angew. Chem., Int. Ed.*, 2017, **56**, 6473–6477.
118 Nonappa and P. Engelhardt, *Imaging Microsc.*, 2019, **21**, 22–24.
119 Nonappa, *Beilstein J. Nanotechnol.*, 2020, **11**, 533–546.
120 (*a*) C. Eggeling, J. Widengren, R. Rigler and C. A. M. Seidel, *Anal. Chem.*, 1998, **13**(70), 2651–2659; (*b*) B. A. Kairdolf, A. M. Smith, T. H. Stokes, M. D. Wang, A. N. Young and S. Nie, *Ann. Rev. Chem.*, 2013, **6**, 143–162; (*c*) M. Montalti, A. Cantellia and G. Battistellia, *Chem. Soc. Rev.*, 2015, **44**, 4853–4921; (*d*) Y. Wang and A. Hu, *J. Mater. Chem. C*, 2014, **2**, 6921–6939.
121 (*a*) Y. Pan, S. Neuss, A. Leifert, M. Fischler, F. Wen, U. Simon, G. Schmid, W. Brandau and W. Jahnen-Dechent, *Small*, 2007, **3**, 1941; (*b*) A. Woźniak, A. Malankowska, G. Nowaczyk, B. F. Grześkowiak, K. Tuśnio, R. Słomski, A. Zaleska-Medynska and S. Jurga, *J. Mater. Sci.: Mater. Med.*, 2017, **28**, 92.
122 (*a*) N. Goswami, F. Lin, Y. Liu, D. T. Leong and J. Xie, *Chem. Mater.*, 2016, **28**(11), 4009–4016; (*b*) N. Goswami, Q. Yao, Z. Luo, J. Li, T. Chen and J. Xie, *J. Phys. Chem. Lett.*, 2016, **7**(6), 962–975; (*c*) D. Bera and N. Goswami, *J. Phys. Chem. Lett.*, 2021, **12**, 9033–9046.
123 J. M. Forward, D. Bohmann, J. P. Fackler, Jr. and R. J. Staples, *Inorg. Chem.*, 1995, **34**, 6330–6336.
124 Y. Huang, L. Fuksman and J. Zheng, *Dalton Trans.*, 2018, **47**, 6267–6273.
125 H. Schmidbaur, *Gold Bull.*, 1990, **23**, 11–21.
126 S.-H. Cha, J.-U. Kim, K.-H. Kim and J.-C. Lee, *Chem. Mater.*, 2007, **19**, 6297–6303.
127 G. A. Palermo, M. Tarannum and S. Egusa, *J. Phys. Chem. C*, 2020, **124**, 11248–11255.
128 Y. Huang, L. Fuksman and J. Zheng, *Dalton Trans.*, 2018, **47**, 6267–6273.
129 D. Bera, M. Baruah, A. K. Dehury, A. Samanta, Y. S. Chaudhary and N. Goswami, *J. Phys. Chem. Lett.*, 2022, **13**, 9411–9421.
130 S. Chandra, Nonappa, G. Beaune, A. Som, S. Zhou, J. Lahtinen, H. Jiang, J. V. I. Timonen, O. Ikkala and R. H. A. Ras, *Adv. Opt. Mater.*, 2019, **7**, 1900620.
131 H. Chen, L. Shao, Q. Lia and J. Wang, *Chem. Soc. Rev.*, 2013, **42**, 2679–2724.
132 A. M. Alkilany, L. B. Thompson, S. P. Boulos, P. N. Sisco and C. J. Murphy, *Adv. Drug. Delivery Rev.*, 2012, **64**, 190–199.
133 H. Yu, Y. Peng, Y. Yang and Z.-Y. Li, *npj Comput. Mater.*, 2019, **5**, 45.
134 H.-X. Xia, X.-Q. Yang, J.-T. Song, J. Chen, M.-Z. Zhang, D.-M. Yan, L. Zhang, M.-Y. Qin, L.-Y. Bai, Y.-D. Zhao and Z.-Y. Ma, *J. Mater. Chem. B*, 2014, **2**, 1945–1953.
135 A. Chakraborty, A. C. Fernandez, A. Som, B. Mondal, G. Natarajan, G. Paramasivam, T. Lahtinen, H. Häkkinen, Nonappa and T. Pradeep, *Angew. Chem., Int. Ed.*, 2018, **57**, 6522–6526.
136 A. Chakraborty, M. M. Stanley, B. Mondal, Nonappa, M. Bodiuzzaman, P. Chakraborty, M. P. Kannan and T. Pradeep, *Nanoscale*, 2023, **15**, 2690–2699.
137 P. Bose, P. Chakraborty, J. S. Mohanty, Nonappa, A. R. Chowdhuri, E. Khatun, T. Ahuja, A. Mahendranath and T. Pradeep, *Nanoscale*, 2020, **12**, 22116–22128.
138 J. Roy, B. Mondal, G. Vishwakarma, Nonappa, N. V. Sridharan, P. Krishnamurthi and T. Pradeep, *Nanoscale*, 2023, **15**, 8225–8234.
139 P. Reineck, D. Gómez, S. H. Ng, M. Karg, T. Bell, P. Mulvaney and U. Bach, *ACS Nano*, 2013, **7**(8), 6636–6648.
140 A. Chakraborty, H. Dave, B. Mondal, Nonappa, E. Khatun and T. Pradeep, *J. Phys. Chem. B*, 2022, **126**, 1842–1851.
141 J. V. Rival, Nonappa and E. S. Shibu, *ACS Appl. Mater. Interfaces*, 2020, **12**, 14569–14577.
142 (*a*) W. C. Wimley, *Curr. Opin. Struct. Biol.*, 2003, **13**, 404–411; (*b*) I. S. Park, Y. R. Yoon, M. Jung, K. Kim, S. Park, S. Shin, Y. B. Lim and M. Lee, *Chem. – Asian J.*, 2011, **6**, 452–458; (*c*) N. A. Yewdall, T. M. Allison, F. G. Pearce, C. V. Robinson and J. A. Gerrard, *Chem. Sci.*, 2018, **9**, 6099–6106; (*d*) C. Du, Z. Li, X. Zhu, G. Ouyang and M. Liu, *Nat. Nanotechnol.*, 2022, **17**, 1294–1302.
143 K. M. Lakshmi, J. V. Rival, S. R. Nambiar, P. Sreeraj, C. Jeyabharathi, Nonappa and E. S. Shibu, *Small*, 2023, **19**, 2207119.
144 (*a*) J. Majoinen, J. Hassinen, J. S. Haataja, H. T. Rekola, E. Kontturi, M. A. Kostiainen, R. H. A. Ras, P. Törmä and O. Ikkala, *Adv. Mater.*, 2016, **28**, 5262–5267; (*b*) A. Chakraborty, Nonappa, B. Mondal,

K. Chaudhari, H. Rekola, V. Hynninen, M. A. Kostiainen, R. H. A. Ras and T. Pradeep, *J. Phys. Chem. C*, 2021, **125**, 3256–3267.
145 N. Mohammed, A. Baidya, V. Murugesan, A. A. Kumar, M. A. Ganayee, J. S. Mohanty, K. C. Tam and T. Pradeep, *ACS Sustain. Chem. Eng.*, 2016, **4**, 6167–6176.
146 (*a*) V. Hynninen, S. Hietala, J. R. McKee, L. Murtomäki, O. J. Rojas, O. Ikkala and Nonappa, *Biomacromolecules*, 2018, **19**, 2795–2804; (*b*) V. Hynninen, P. Mohammadi, W. Wagermaier, S. Hietala, M. B. Linder, O. Ikkala and Nonappa, *Eur. Polym. J.*, 2019, **112**, 334–345; (*c*) V. Hynninen, J. Patrakka and Nonappa, *Materials*, 2021, **14**, 5137.
147 V. Hynninen, S. Chandra, S. Das, M. Amini, Y. Dai, S. Lepikko, P. Mohammadi, S. Hietala, R. H. A. Ras, Z. Sun, O. Ikkala and Nonappa, *Small*, 2021, **17**, 2005205.
148 S. Chandra, A. Sciortino, S. Shandilya, L. Fang, X. Chen, Nonappa, H. Jiang, L.-S. Johansson, M. Cannas, J. Ruokolainen, R. H. A. Ras, F. Messina, B. Peng and O. Ikkala, *Adv. Opt. Mater.*, 2023, **11**, 2201901.